PONTIFICIA UNIVERSIDAD CATOLICA DE CHILE
SCHOOL OF ENGINEERING

MODELING OXYGEN DISSOLUTION DURING PULSE OXYGEN ADDITIONS UNDER OENOLOGICAL CONDITIONS

PEDRO ANDRÉS E. SAA HIGUERA

Thesis submitted to the Office of Research and Graduate Studies in partial fulfillment of the requirements for the Degree of Master of Science in Engineering

Advisor:
J. RICARDO PÉREZ-CORREA

Santiago de Chile, October, 2012

PONTIFICIA UNIVERSIDAD CATOLICA DE CHILE
SCHOOL OF ENGINEERING

MODELING OXYGEN DISSOLUTION DURING PULSE OXYGEN ADDITIONS UNDER OENOLOGICAL CONDITIONS

PEDRO ANDRÉS E. SAA HIGUERA

Members of the Committee:

RICARDO PÉREZ-CORREA

DIEGO CELENTANO

EDUARDO AGOSIN

FRANCISCO CUBILLOS

PABLO PASTÉN

Thesis submitted to the Office of Research and Graduate Studies in partial fulfillment of the requirements for the Degree of Master of Science in Engineering

Santiago de Chile, October, 2012

Gratefully to my parents, Pedro and Haydee, my brother Diego and especially to you Claudia, who have supported me throughout this work

ACKNOLEDGEMENTS

First, I would like to thank my family and friends for the unconditional support during the preparation of this work. Without you, this task would not been possible. I would also like to thank Isabel and Martin for their time, patience and collaboration during the experiments and to everyone who contributed in numerous ways to make this work possible. I am particularly grateful to my advisor, Ricardo, and to the professors, Eduardo and Claudio, for stimulating my development as biochemical engineer during the last years.

Finally, I would like to extend my gratitude to the National Fund for Scientific and Technological Development of Chile (FONDECYT) No. 1090520 for its economic support during the realization of this work.

TABLE OF CONTENTS

Pág.

ACKNOLEDGEMENTS iii

LIST OF TABLES vii

LIST OF FIGURES viii

ABSTRACT ix

RESUMEN xi

1. INTRODUCTION 13
   - 1.1 Background 14
     - 1.1.1 Gas-Liquid oxygen mass transfer 16
     - 1.1.2 Biological consumption of dissolved oxygen 18
     - 1.1.3 Oxygen management during winemaking 19
     - 1.1.4 Oxygen additions during fermentation 20
   - 1.2 Goals 21
   - 1.3 Hypothesis 22
   - 1.4 Methodology 23
     - 1.4.1 Oxygen dissolution and uptake under oenological conditions on laboratory scale 23
     - 1.4.2 Impact of carbon dioxide on the oxygen dissolution during pulse additions 24

2. RESULTS AND CONCLUSIONS 25
   - 2.1 Future perspectives 26

A P P E N D I X 27

APPENDIX A: MODELING OXYGEN DISSOLUTION AND BIOLOGICAL UPTAKE DURING PULSE OXYGEN ADDITIONS IN OENOLOGICAL FERMENTATIONS 28
A.1 Abstract 28
A.2 Introduction 29
A.3 Model development 33
A.3.1 Oxygen mass balance 34
A.3.2 Oxygen solubility 35
A.4 Materials and Methods 37
A.4.1 Yeast strain 37
A.4.2 Culture media and fermentation conditions 37
A.4.3 Analytical techniques 38
A.4.4 Oxygen additions 38
A.4.5 Dissolved oxygen 38
A.4.6 Oxygen solubility 39
A.4.7 k_La measurements in synthetic solution 39
A.4.8 Parameter fitting 40
A.4.9 Regression diagnostics 42
A.5 Results and discussion 42
A.5.1 Calibration of the oxygen solubility model 42
A.5.2 Oxygen uptake rate model calibration under perfect mixing conditions 45
A.5.3 Comparison of experimental results and model predictions 48
A.5.4 Oxygen uptake rate model calibration under non- agitated conditions 53
A.5.5 Influence of agitation conditions upon the oxygen uptake response time 53
A.5.6 Oxygen mass transfer under oenological conditions 56
A.5.7 Influence of the dissolved carbon dioxide upon the mass transfer coefficient 58
A.6 Conclusions 58

APPENDIX B: IMPACT OF CARBON DIOXIDE INJECTION ON OXYGEN DISSOLUTION RATE DURING OXYGEN PULSE ADDITIONS IN A BUBBLE COLUMN 60
B.1 Abstract 60
B.2 Introduction 61
B.3 Modeling 64
B.3.1 Oxygen mass balance model 65
B.3.2 Hydrodynamics 66
B.3.3 Gas hold-up and axial dispersion coefficient prediction 68
B.3.4 Oxygen solubility estimation 69
B.4 Materials and Methods 69
B.4.1 Experimental set-up 69
B.4.2 Oxygen pulse additions and k_La determination 71
B.4.3 Oxygen solubility 72
B.4.4 Numerical resolution 73
B.4.5 Parameter fitting 73
B.4.5 Statistics 74
B.5 Results and discussion 74
B.5.1 Oxygen saturation concentration with simultaneous carbon dioxide injection 74
B.5.2 Oxygen dissolution during oxygen additions without carbon dioxide injection 75
B.5.3 Oxygen dissolution during oxygen additions with carbon dioxide injection 78
B.5.4 Influence of simultaneous carbon dioxide injection on the oxygen dissolution rate 82
B.6 Conclusions 84

REFERENCES 85

LIST OF TABLES

Pág.

Table A-1: Fitted parameters of the oxygen solubility model for temperatures ranging between 15 and 37°C 44

Table A-2: Validation of the oxygen solubility model at 25°C 45

Table A-3: Comparison of the different models 47

Table B-1: Oxygen solubility using different carbon dioxide flows at 20°C 74

Table B-2: Fitted and predicted $k_L a$ under the studied conditions 81

Table B-3: Comparison of different oxygen dissolution terms 83

LIST OF FIGURES

Pág.

Figure A-1: A typical absorption-desorption cycle occurring during an oxygen impulse under oenological conditions 41

Figure A-2: Time-dependent normalized sensitivities of the OUR parameters model during the experiment 47

Figure A-3: Oxygen uptake rate model for different biomass concentrations during oenological fermentations 49

Figure A-4: Specific oxygen consumption kinetics by *Saccharomyces cerevisiae* and increase of the parameter *n* with the biomass concentration 50

Figure A-5: Specific oxygen uptake rate optimization and biomass growth 52

Figure A-6: Comparison of different oxygen consumption dynamics for different hydrodynamic conditions 54

Figure A-7: Oxygen mass transfer under oenological conditions 57

Figure B-1: Details of the experimental set-up 71

Figure B-2: Kinetics of oxygen dissolution without carbon dioxide injection at different positions throughout the column 76

Figure B-3: Kinetics of oxygen dissolution with 350 mL min^{-1} carbon dioxide injection at different positions throughout the column 79

Figure B-4: Kinetics of oxygen dissolution with 700 mL min^{-1} carbon dioxide injection at different positions throughout the column 80

ABSTRACT

During industrial wine fermentations, discrete oxygen additions are a common practice to increase the fermentation rate. However, the oxygen dose and time must be carefully chosen to avoid detrimental effects on wine quality. So far, current additions are performed mostly empirically, since oxygen dissolution under oenological conditions is not completely understood. Thus, to efficiently manage oxygen additions, this work presents two oxygen mass balance models able to reproduce the oxygen dissolution evolution during pulse additions in wine fermentations on a laboratory scale and in abiotic conditions emulating fermentation in a bubble column. Model results on a laboratory scale indicated that the specific oxygen uptake rate of the *Saccharomyces cerevisiae* wine strain strongly depends on the growth phase and that the oxygen mass transfer coefficient is modified by the biological uptake. Results also indicated that the agitation has a significant effect on the oxygen uptake rate and confirmed the negative effect of carbon dioxide on the oxygen transfer rate. Model predictions in the bubble column showed that the carbon dioxide bubbling enhances the volumetric mass transfer coefficient due to the increased gas superficial velocity and induced turbulence, but also decreases the oxygen solubility because of the large dilution effect of oxygen in the gas phase. Overall, experimental and model results showed that carbon dioxide presence decreases the oxygen dissolution rate in about half compared with the case without carbon dioxide injection. The developed models will provide better tools for managing oxygen additions and for designing better addition systems for industrial wine fermentations.

Keywords: Oxygen dissolution, oxygen uptake, mass transfer coefficient, wine fermentation, modeling

RESUMEN

Durante fermentaciones enológicas industriales, adiciones discretas de oxígeno son una práctica común para aumentar la tasa de fermentación. Sin embargo, la dosis de oxígeno y el tiempo de la adición deben ser escogidos cuidadosamente para evitar efectos perjudiciales en la calidad del vino. Hasta ahora, las adiciones se llevan a cabo de manera empírica, ya que aún no se entiende completamente la dinámica de disolución del oxígeno en condiciones enológicas. Por lo tanto, para administrar eficientemente las adiciones de oxígeno, en este trabajo se presentan dos modelos de balance de masa de oxígeno capaces de reproducir la evolución de la disolución durante pulsos de adición en fermentaciones enológicas a escala de laboratorio y en condiciones abióticas emulando fermentaciones en una columna de burbujeo. Calibraciones del modelo a escala de laboratorio indican que la tasa específica de consumo de oxígeno de *Saccharomyces cerevisiae* depende fuertemente de la fase de crecimiento y que el coeficiente de transferencia de masa es influenciado por el consumo biológico. Los resultados también indican que la agitación tiene un efecto significativo en la tasa de consumo y confirman el efecto negativo de los altos niveles de dióxido de carbono en la transferencia de oxígeno. Predicciones del modelo en la columna de burbujeo muestran que la presencia de dióxido de carbono aumenta el coeficiente de transferencia de masa debido al aumento de la velocidad superficial del gas y a la turbulencia inducida, pero también disminuye la solubilidad del oxígeno debido al efecto de dilución en la fase gaseosa. En definitiva, el dióxido de carbono disminuye la tasa de disolución del oxígeno en aproximadamente la mitad en comparación con el caso sin inyección de dióxido de carbono. Los modelos desarrollados brindarán mejores

herramientas para la gestión de las adiciones de oxígeno y para el diseño de mejores sistemas de adición para fermentaciones enológicas industriales.

Palabras claves: Disolución de oxígeno, consume de oxígeno, coeficiente de transferencia de masa, fermentación enológica, modelamiento

1. INTRODUCTION

The present work will focus on understanding the oxygen phenomenon during wine fermentations. The aim of this study is to develop useful models and tools that enable winemakers to manage oxygen additions in a more rational manner during oenological fermentations. The latter will help reducing detrimental effects on wine quality due to poorly managed additions and exploiting the benefits of precise oxygen doses on the development of desired aromas and on the stabilization of the resulting wine colour.

Despite the importance of oxygen addition during the fermentation process, there are until now no systematic studies that assess the impact of oenological conditions upon the oxygen dissolution and the specific biological uptake. The physicochemical equilibrium of oxygen in solutions similar to fermenting musts and wine is still not fully understood, in spite of many isolated data. The latter is essential to properly describe and quantify the oxygen mass transfer rate. The evolution of the yeast specific oxygen uptake is also important as the biological uptake is known to enhance the oxygen mass transfer (Merchuk, 1977; Garcia-Ochoa et al., 2000, 2010). When modeling the oxygen dissolution, the impact of carbon dioxide production during wine fermentation is also of interest, as it negatively affects the oxygen solubility due to the dilution effect of oxygen in the gas phase (Devatine et al., 2007; Devatine and Mietton-Peuchot, 2009; Chiciuc et al., 2010). Nevertheless, the effect of the naturally produced carbon dioxide bubbles on the oxygen mass transfer, *e.g.* on the volumetric mass transfer coefficient, so far has not been assessed

despite the relative high production rates observed during wine fermentations. Overall, understanding the oxygen dissolution during wine fermentations involves a complete study of the many factors that influence the dissolution. The above is the main goal of this thesis.

The present work is organized on the basis of two scientific papers soon to be submitted or already published in specialized journals. Both papers address different factors influencing oxygen dissolution in different scales and are included in the appendix of this manuscript. In Appendix A, the article "*Modeling oxygen dissolution and biological uptake during pulse oxygen additions in oenological fermentations*" submitted, accepted and recently published in the Bioprocess and Biosystems Engineering Journal is shown. The second article called "*Impact of carbon dioxide injection on oxygen dissolution rate during oxygen pulse additions in a bubble column*" is shown in Appendix B. This paper will be soon submitted to a specialized Chemical Engineering Journal for its publication. The first and second chapters of this work are intended to present an introduction to the topic and outline the main results of this work, respectively. Altogether, they provide an integrative and global view of the work done.

1.1 Background

Oxygen can make or break wines. Indeed, winemakers are aware that oxygen is a critical factor to consider over the whole winemaking process. From a microbial perspective, it allows the yeast to synthesize those "anaerobic" growth factors – ergosterol and oleic acid - required to ensure cell viability at the later stages of the fermentation, *i.e.* under increasing ethanol content. From the chemical side, its addition could result in

softer, even more aromatic, colour-stable wines. However, wine oxidation and oxidative degradation of precious aromatic compounds could easily take over if oxygen dissolution is not carefully managed during the whole process.

In wine production, oxygen is always encountered. From the moment of harvest or during operations such as crushing, pressing, racking and fermentation, oxygen will be present. The consequences of significant oxygen exposure range from notorious flavor changes to acetification (Oszmianski et al., 1996; Pyrzyńska, 2004; Ribéreau-Gayon et al., 2006). To manage this problem, many technological solutions have been implemented, such as those that can minimize the contact with air (*e.g.* blanketing with inert gases) and those that make oxidation less apparent (*e.g.* the use of sulfur dioxide in the binding of aldehydes). Conversely, moderate oxygen exposure could benefit some wines by, for instance, improving yeast performance and contributing to the aromatic diversity, stabilization of colour and reduction of astringency and bitterness (Atanasova et al., 2002; Castellari et al., 2004). Thus, the optimal management of oxygen incorporation during the winemaking process is essential to produce a high quality product.

Optimal management of oxygen requires setting up a dynamic mass balancing during fermentation, which could be represented by the following expression,

$$\frac{d\mathrm{O}_2}{dt} = Q_g - q_{\mathrm{O}_2} \cdot X - \Psi \qquad (1.1)$$

where Q_g is the volumetric oxygen transfer rate; q_{O2} , the specific oxygen consumption rate of the yeast; X, the total biomass in the fermenter and Ψ, the sum of all abiotic reactions

of oxygen. The latter term will not be treated here, since the biological oxygen consumption is far more important than chemical consumption during wine fermentation.

1.1.1 Gas-Liquid oxygen mass transfer

The oxygen transfer rate from a gas phase to a liquid phase in a bubbled liquid tank is usually estimated by (Villadsen et al., 2011),

$$Q_g = k_L a \cdot \left(O_2^* - O_2 \right) \qquad (1.2)$$

where $k_L a$ is the volumetric mass transfer coefficient; O_2^*, the saturation concentration of oxygen in the liquid phase and O_2 denotes the oxygen concentration in the bulk liquid. Oxygen solubility depends on temperature, oxygen partial pressure in the gas phase, pH and concentrations of ethanol, glucose and fructose in the fermenting must or wine (Singleton, 1987; Chiciuc et al., 2010). At room temperature and atmospheric pressure, oxygen solubility with air reaches a maximum in wine at about 6 or 8 mg L^{-1}. If the wine is exposed to high doses of pure oxygen instead, such as during micro-oxygenation, saturation levels of 30 mg L^{-1} would be expected (Singleton 2000). In simple models, the saturation concentration in diluted solutions can be estimated using Henry's law,

$$O_2^* = \frac{p_{O_2}^*}{H} \qquad (1.3)$$

where $p_{O_2}^*$ is the partial pressure of the solute gas in the gas phase and H is the Henry's constant for the given gas. For oxygen and carbon dioxide in water at 25 ºC, the values of H (790 and 29.7 atm L $mole^{-1}$, respectively) can be used for a quick estimation of their solubility in wine. It can be seen that carbon dioxide is much more soluble than oxygen,

which help explaining its negative effect on the oxygen mass transfer. Indeed, experiments carried out by Devatine et al. (2007) showed that the dissolved carbon dioxide decreases dramatically the oxygen transfer performance. Thus, the carbon dioxide is of great importance when quantifying the oxygen transfer.

On the other hand, the rate upon oxygen in transferred to the liquid phase depends on the volumetric mass transfer coefficient, $k_L a$. Estimating and even measuring $k_L a$ is much more difficult than determining the oxygen solubility. Although a large number of empirical correlations of $k_L a$ for a variety of bioreactor designs with (Moo-Young and Blanch, 1981; Lemoine et al., 2008; Villadsen et al., 2011) or without (Linek et al., 2005) mechanical agitation have been proposed, it is not clear if these correlations are applicable to oxygen addition during wine fermentation. Indeed, in this case there are two gas streams, the added air (or pure oxygen) and the carbon dioxide released during fermentation. Therefore, adaptation of the existing correlations to this situation may be difficult, so measuring $k_L a$ under oenological conditions may be unavoidable to properly estimate the oxygen mass transfer.

The most common techniques to measure $k_L a$ are the conventional gassing in and gassing out dynamic methods (Taguchi and Humphrey, 1966). The interpretation of the dissolved gas evolution to estimate $k_L a$ may be difficult, since these estimations depend on the time response, location of the probe and the liquid hydrodynamics, as well as the model used to interpret the recorded data (Gourich et al., 2008). The simplest model that yields reproducible $k_L a$ values for small well agitated vessels is the perfect stirred tank with

sensor dynamics model. For larger tanks, without mechanical agitation, like micro-oxygenation during wine aging, a plug flow model for the gas phase and axial dispersion model for the liquid phase is more appropriate (Dhaouadi et al., 2008).

Systematic studies to measure k_La during wine fermentation are scarce. Blateyron et al. (1998) computed the k_La for a 500 L tank and found almost constant values for sugar concentrations above 70 g L^{-1}. In their calculations they considered perfect mixing, no sensor dynamics and that oxygen solubility depends on sugar concentration only. Devatine et al. (2007), using an experimental bubble column and a fast sensor, found that k_La values, computed with the perfectly stirred tank model, strongly depends on the carbon dioxide concentration in the wine. Since the carbon dioxide dissolved in the liquid is transferred to the gas phase as it moves up the column, the oxygen partial pressure is reduced, therefore reducing oxygen solubility. Hence, a simple perfectly stirred model where the oxygen balance in the gas phase is neglected is no longer applicable. In summary, reliable methods of wide applicability to compute k_La values during wine fermentation are still to be developed.

1.1.2 Biological consumption of dissolved oxygen

Yeasts are unable to grow well in the complete absence of oxygen. This is because, as well as providing a substrate for respiratory enzymes during aerobic growth, oxygen is required for certain growth-maintaining hydroxylations, such as those involving the biosynthesis of sterols and unsaturated fatty acids, *e.g.* ergosterol and oleic acid (Salmon,

2006). The latter are an absolute requirement for *Saccharomycces cerevisiae* to grow during the fermentation (Rosenfeld et al., 2002).

Oxygen should therefore be regarded as an important yeast growth factor (Walker, 1998). Oxygen requirement is low and has been estimated to be in the order of 1.5 to 3.5 mg per g of yeast dry weight for enological fermentations (Rosenfeld et al., 2003). The choice of the moment in which oxygen must be added is as important as the quantity. Oxygen is apparently more effective if the addition is made at the growing phase end, when the carbon dioxide production is the highest; however, the addition is still effective until half of the fermentation (Sablayrolles and Barre, 1986; Blateyron et al., 1998). Nevertheless, during these phases the *S. cerevisiae* wine strain shows different specific oxygen uptake rates (Sablayrolles et al., 1996), which implies that to accurately quantify the oxygen uptake it must be done at the proper time and under the right conditions.

1.1.3 Oxygen management during winemaking

The use of commercial devices to introduce small amounts of oxygen during and after alcoholic fermentation, generally called micro-oxygenation, is common practice in many wineries (Salmon, 2006). The main benefits of this technique in wine are the elimination of vegetal and sulphide aromas, and an improvement in colour stability and "tannin structure" (Miller, 2001; Rieger, 2000; Zoecklein 2000; Parish 2000). The general principle of micro-oxygenation is the addition of small amounts of oxygen into the wine by means of a sparger that distributes the gas in the form of small bubbles (Zoecklein 2000, Miller 2001, Parish 2000, Rieger 2000, Rowe 1999). However, adding too much oxygen is

deleterious to wine quality, but in low doses is ineffective. Therefore, it is important to measure and control these additions.

Controlled oxygen additions during wine fermentations can be beneficial, too. Blateyron and Sablayrolles (2001) and Sablayrolles et al. (1996) have shown that adding nitrogen and oxygen at the halfway point of the fermentation, completely avoids sluggish and stuck fermentations. In addition, Valero et al. (2002) compared the higher alcohols and esters content of wines fermented with and without oxygenated musts. They found higher aroma contents in wines from oxygenated musts, although with a lower esters/higher-alcohols ratio. Moreover, oxygen additions during wine fermentation significantly reduce the oxygen consumption rates and total capacity of oxygen consumption by the corresponding yeast lees (Salmon, 2006).

1.1.4 Oxygen additions during fermentation

There are basically two systems to add small controlled amounts of oxygen to wine, bubbling through spargers and diffusion through membranes. Blateyron et al. (1998) tested both systems in lab scale (1.2 and 2 L) and pilot scale (500 and 3000 L) vessels during wine fermentation. In the membrane system, the wine was circulated inside a silicone tube which in turn was submerged in a sealed jar containing an oxygen saturated solution. On the other hand, in the bubbling system the sparger was installed in the vessel or in a wine circulation loop; both systems worked well. Silva and Lambri (2006) also applied oxygen during fermentation in 6000 L tanks. They tested two sparger systems, one that operated during pumping-over and the other that operated during must recirculation.

Both methods achieved adequate oxygenation, although the must recirculation method was faster reaching higher dissolved oxygen values of 5.5 mg L^{-1}.

Oxygen additions during winemaking are punctual or continuous flow, but in both cases dissolved oxygen levels are not controlled, only measured. However, Burke et al. (1998) have shown that dissolved oxygen in yeast cultures can be controlled precisely at very low levels in 3.5 L fermenters. Using a simple feedback control and a perfect stirred tank model, they were able to control oxygen levels in the range of 6 µg L^{-1} to 6 mg L^{-1} with a deviation of ±3 µg L^{-1}, i.e., in the low range of dissolved oxygen values found during wine fermentation. Moreover, oxygen levels could be adjusted to new values within 4 min. However, this type of control system cannot be implemented for controlling dissolved oxygen at industrial scale, because of the limitations of the perfect stirred tank model. Thus, oxygen dissolution models on a larger scale under oenological conditions are still to be developed for managing oxygen additions.

1.2 Goals

The main goal of this work is to develop useful models that allows studying and reproducing the dynamics of dissolved oxygen under conditions similar to those encountered during wine fermentation. The following are the specific objectives considered in this goal:

1. To develop a model to estimate the solubility of oxygen in multicomponent hydroalcoholic solutions, similar to fermenting musts.

2. To develop a dynamic oxygen dissolution and biological consumption model that allows reproducing the short term response following oxygen pulses during fermentations at laboratory scale.
3. To design and implement an experimental bubble column that allows studying and modeling oxygen dissolution under conditions resembling oenological industrial fermentations.
4. To experimentally validate the developed models under the studied conditions.

1.3 Hypothesis

The development of useful models that reproduces the dissolved oxygen kinetics in conditions similar to those encountered during wine fermentation, will lead to a better understanding of the key variables governing this process, allowing to optimize the additions in opportunity and amount.

1.4 Methodology

The general methodologies adopted to achieve the specific objectives of this work are divided in two on the basis of the two scientific papers written. The details of each methodology can be revised in Appendix A.4 and B.4, respectively.

1.4.1 Oxygen dissolution and uptake under oenological conditions on laboratory scale

First, a model for oxygen solubility considering the effect of sugar, ethanol and temperature, based on the "log-additivity" law will be developed, using the data of Kutsche et al. (1984), Mishima et al. (1996) and Eya et al. (1994), among others. Then, model predictions will be compared with measurements of dissolved oxygen using a high accuracy optical sensor 3 LCD-trace Fibox v7 (PreSens®, Regensburg, Germany) at different temperatures and oxygen saturation levels by sparging the medium with either pure oxygen or air.

Then, the kinetics of microbial oxygen consumption and oxygen dissolution at different stages of wine fermentation will be studied. The *Saccharomyces cerevisiae* EC1118, an industrial yeast strain widely used by the wine industry will be grown in a modified MS300 medium (Salmon and Barre, 1998), a defined culture medium emulating the components of grape juice, at 25 °C and pH 3.5. The effect of the fermentation stage on the specific oxygen consumption rate of yeast cells, q_{O2}, will be determined as follows: after reaching the end of the growth phase, a pulse of oxygen will be applied to the fermentation culture. The amount and duration of the oxygen pulse will be estimated in

order to reach dissolved oxygen amounts of around 3 to 5 mg L^{-1}. The fate of dissolved oxygen will be followed online and *in situ* with the above mentioned optical sensor. Uptake kinetic parameters and the volumetric mass transfer coefficient (responsible for the oxygen dissolution) will then be calculated for each culture, and kinetic expressions for oxygen uptake rates during fermentation will be developed.

1.4.2 Impact of carbon dioxide on the oxygen dissolution during pulse additions

Gaseous and dissolved carbon dioxide significantly affects oxygen transfer from the gas to the liquid phase (Devatine et al., 2007). So, its impact on the oxygen transfer rate coefficient, $k_L a$, in abiotic conditions will be assed. For this purpose, a bubble column of 1.5 m height and 0.3 m diameter will be set up; where different porous diffusers inserted at the bottom will emulate the hydrodynamics caused by the carbon dioxide bubbling. Different carbon dioxide bubbling rates (from 0 to 0.9 g L^{-1} h^{-1}), emulating the carbon dioxide production rates observed during wine fermentation (Casalta et al., 2010), will be evaluated. $k_L a$ values will be estimated using the dynamic method and a distributed parameter model developed in this work.

2. RESULTS AND CONCLUSIONS

The results of this work are of interest as they cover an important aspect of winemaking that has been poorly studied: oxygen addition. The novel methodology developed and employed for describing the oxygen dissolution kinetics following an oxygen pulse on laboratory scale wine fermentations, allowed to accurately quantify the biological consumption rate and to assess its influence on the oxygen mass transfer. Model calibrations on laboratory scale showed that the specific oxygen uptake rate of the *S. cerevisiae* wine strain varies along the fermentation course, reaching a maximum at the end of the growth phase. Results also indicated that the volumetric mass transfer coefficient is positively influenced by the biological uptake increasing from 5.14 to 13.43 h^{-1}, when oxygen uptake rate increased from 20 to 108 mg O_2 L^{-1} h^{-1}. Regarding the influence of the agitation condition on the biological uptake, model estimations showed that it has a significant effect on both the oxygen consumption response time and the shape of the response curve. The negative effect of high levels of carbon dioxide upon the mass transfer coefficient was also confirmed experimentally, although the oxygen stripping due to carbon dioxide bubbles was found to be negligible during the biological uptake.

In the case of the bubble column experiments, the proposed distributed parameter model reproduced fairly well the dissolved oxygen profiles observed during the oxygen additions. Model and experimental results showed that the carbon dioxide injection increases the estimated volumetric mass transfer coefficient value, but also reduces dramatically the oxygen solubility in the liquid phase, as it dilutes the oxygen fraction in

the gas phase. Model predictions showed that carbon dioxide injection increases the volumetric mass transfer coefficient from $3.5 \cdot 10^{-4}$ to $7.2 \cdot 10^{-4}$ s^{-1} for maximum carbon dioxide injection rate, but simultaneously reduces the oxygen solubility in the liquid phase by 80%, as it dilutes the oxygen fraction in the gas phase. The latter effect has shown to be more important, as the observed oxygen dissolution rate decreased more than 60% compared to the case with no carbon dioxide presence.

Overall, the results of this thesis indicate that several factors, such as the fermentation phase, wine composition, mixing and carbon dioxide content, must be considered when performing oxygen additions during oenological fermentations, being the carbon dioxide presence one of the most important factors influencing the oxygen dissolution phenomenon.

2.1 Future perspectives

The results of this work will help developing better oxygen additions policies during wine fermentation according to the biological needs. The distributed oxygen dissolution parameter model developed here will help in the design of better oxygen delivery systems for industrial wine fermentations. Furthermore, this model could be further improved and implemented for controlling dissolved oxygen concentration at industrial scale during oenological fermentations. The latter will allow developing novel control systems for managing oxygen additions during wine fermentations.

APPENDIX

APPENDIX A: MODELING OXYGEN DISSOLUTION AND BIOLOGICAL UPTAKE DURING PULSE OXYGEN ADDITIONS IN OENOLOGICAL FERMENTATIONS

A.1 Abstract

Discrete oxygen additions during oenological fermentations can have beneficial effects both on yeast performance and on the resulting wine quality. However, the amount and time of the additions must be carefully chosen to avoid detrimental effects. So far, most oxygen additions are carried out empirically, since the oxygen dynamics in the fermenting must are not completely understood. To efficiently manage oxygen dosage, we developed a mass balance model of the kinetics of oxygen dissolution and biological uptake during wine fermentation, on a laboratory scale. Model calibration was carried out employing a novel dynamic desorption-absorption cycle based on two optical sensors able to generate enough experimental data for the precise determination of oxygen uptake and volumetric mass transfer coefficients. A useful system for estimating the oxygen solubility in defined medium and musts was also developed and incorporated into the mass balance model. Results indicated that several factors, such as the fermentation phase, wine composition, mixing and carbon dioxide concentration, must be considered when performing oxygen addition during oenological fermentations. The present model will help develop better oxygen addition policies in wine fermentations on an industrial scale.

A.2 Introduction

Wine fermentation is an anaerobic bioprocess. However, discrete oxygen additions are common practice in most wineries because they favor fermentation kinetics and biomass formation (Fornairon-Bonnefond et al., 2002), and are beneficial to aroma diversity and color stability (Salmon, 2006; Pérez-Magariño et al., 2007). Yeast cells have an absolute requirement for oxygen for the synthesis of several intracellular components, particularly sterols and unsaturated fatty acids, which are essential for plasma membrane integrity (Blayteron, L. and Sablayrolles, 2001). Under anaerobiosis, yeasts are able to incorporate grape-derived sterols, which promote initial growth and fermentative activity by substituting ergosterol in the cell membranes. However, if oxygen deficiency is maintained, the rapid accumulation of these phytosterols modifies the physicochemical properties of the yeast cell membrane, leading to sluggish fermentations (Salmon, 2006).

Growth of *Saccharomyces cerevisiae* during alcoholic fermentation requires oxygen concentrations of 5 to 7.5 mg O_2 L^{-1}(Sablayrolles and Barre, 1986; Rosenfeld et al., 2004). Nevertheless, oxygen could also be detrimental when added at the wrong moment or in too high concentrations, resulting in wine oxidation, color degradation and off-flavors synthesis (Adoua et al., 2010). Therefore, the amount and opportunity of oxygenation must be carefully managed to avoid such undesirable effects.

At present, oxygen additions are performed mostly empirically, since the kinetics of oxygen dissolution and oxygen consumption in the fermenting must are still poorly studied. During oxygen additions, oxygen from the air bubbles is transferred through the gas-liquid interface followed by liquid phase diffusion/bulk transport to the cells. Although

this is a multi-step serial transport, in a well dispersed system, the major resistance to oxygen transfer is in the liquid film surrounding the gas bubble (Villadsen et al., 2011). In the case of oxygen, the gas-liquid mass transfer is commonly modeled by the two-film theory of Whitman (Whitman, 1923). According to this theory, the volumetric mass transfer rate of oxygen can be described as the product of a volumetric mass transfer coefficient, k_La, and a driving force, the difference between oxygen equilibrium concentration, O_2^*, and the actual concentration of dissolved oxygen. The oxygen equilibrium concentration depends on several factors such as temperature, oxygen partial pressure in the gas phase, pH and composition of the fermenting must or wine (Singleton, 1987). For instance, at atmospheric pressure and room temperature, when using air, the oxygen saturation in wine is reached at 6 mg L^{-1}; if the saturation is carried out in the same conditions with pure oxygen, levels of 30 mg L^{-1} can be achieved (Singleton, 2000). To the best of our knowledge, and despite many isolated data, there is no systematic study to calculate oxygen solubility in fermenting musts and wine at different temperatures and compositions.

The oxygen transfer rate (OTR) to the liquid phase depends mainly on the k_La coefficient. This coefficient is affected by several factors, *e.g.* oxygen gas flow-rate, temperature, rheological characteristics and composition of the medium and system's turbulence (Garcia-Ochoa et al., 2000; Chiciuc et al., 2010; Jamnongwong et al., 2010; Caşcaval et al., 2011). The last term accounts for the hydrodynamic condition of the culture and it is fundamental for determining the k_La value (Gagnon et al., 1998). In the

case of stirred bioreactors, this term is commonly associated with the energy input of the system, while in the case of bubble columns and airlift reactors it is mainly influenced by the bubbles produced by the gas injection (Villadsen et al., 2011).

Another factor that could influence the estimated k_La value is the biological oxygen uptake (Merchuk, 1977; Ruthiya et al., 2003; Garcia-Ochoa and Gomez, 2009). When absorption with chemical reaction occurs in a liquid, the concentration profiles are disturbed by the chemical reaction causing an increase in the gradient and, consequently, an enhancement of the mass transfer rate. The ratio of such a rate to the rate of absorption without chemical reaction is called the enhancement factor, *E,* (Garcia-Ochoa and Gomez, 2009). This factor is explained by several mechanisms, both physical and chemical, which are mainly influenced by the operation conditions and culture features (Ruthiya et al., 2003). Since oxygen absorption into a fermentation broth is similar to gas absorption accompanied by a chemical reaction, in that dissolved oxygen is consumed by microorganisms while it diffuses from the gas-liquid interface, the mass transfer rate is expected to be enhanced, as compared with pure physical absorption (Merchuk, 1977). The latter is normally observed in cultures with relative high oxygen uptake rate compared to the k_La coefficient. When the k_La coefficient is relatively high, no influence of the biological oxygen uptake can be detected, because the enhancement is relatively small (Garcia-Ochoa and Gomez, 2009).

To determine the k_La under abiotic conditions, the conventional dynamic method is commonly employed (Devatine et al., 2007). In the case of solutions with growing aerobic

microorganisms, the dynamic method based on the technique described by Taguchi and Humphrey (Taguchi and Humphrey, 1966) is preferred. The latter determines simultaneously both, the k_La and the oxygen uptake rate (OUR), by first turning off momentarily the gas inlet and then turning it back on. Casas et al. (2006) proposed a new approach for simultaneous calculation of the volumetric transfer rate and the oxygen consumption rate in pneumatically aerated bioreactors, without interrupting the gas inlet. Instead, a step change in composition of the aeration gas is imposed without altering its flow rate, and thus, without altering the microbial growth. However, in the case of anaerobic processes like wine fermentation, there are no reported methods for systematically determining the k_La and the OUR during fermentation, without affecting its normal course.

Once oxygen is dissolved in the liquid phase, it is immediately consumed by the microorganism (Garcia-Ochoa et al., 2010). The OUR depends on both the biomass concentration and the specific oxygen uptake rate, and therefore changes during the fermentation. In wine fermentation, maximum OUR values up to 18 mg O_2 L^{-1} h^{-1} have been reported at the end of the growth phase, the optimal time for oxygen addition (Sablayrolles et al., 1996). However, the oxygen consumption rate is commonly determined off – line, *i.e.* outside of the bioreactor, after culture sampling, which might not take into account the influence of several factors encountered under oenological conditions, *e.g.* limited mixing or high carbon dioxide concentrations. Moreover, considering the high carbon dioxide production rates observed during the exponential

phase of fermentation - up to 1.2 g L^{-1} h^{-1}, (Casalta et al., 2010; Morakul et al., 2011) - and the low amounts of oxygen added, it can be argued that significant amounts of the added oxygen are not being consumed by the yeast, but are lost due to CO_2 stripping. Hence, oxygen losses by stripping must also be quantified in order to accurately estimate the biological consumption.

In this work, we developed a dynamic oxygen mass balance model to properly describe the kinetics of oxygen dissolution and consumption, during laboratory scale oenological fermentations. We evaluated the quality of the model by applying several regression diagnostics tests, *e.g.* parameter sensitivity (how changes in parameter values affect response variables); parameter identifiability (detection of cross correlation between parameters) and parameter significance (determine parameter confidence intervals). These tests are crucial tools for model validation and optimization, as they allow us to identify the most significant correlations between parameters and to reduce model's uncertainty (Sacher et al., 2011). The current model includes the influence of agitation and medium composition on the oxygen mass transfer and on biological consumption, as well as the impact of CO_2 stripping on the oxygen dynamics.

A.3 Model development

The resulting dynamic, oxygen mass balance model describes the response of oxygen dissolution and consumption kinetics under oenological conditions when an oxygen pulse is applied. The main model assumptions are:

- Liquid film resistance around bubbles controls the overall mass transfer rate (Garcia-Ochoa and Gomez, 2009).
- Dissolved oxygen is immediately consumed by the yeast (Garcia-Ochoa et al., 2010).
- During the addition of oxygen, the bubbles are uniformly distributed in the bioreactor.
- Chemical oxygen consumption is negligible compared to biological consumption.

A.3.1 Oxygen mass balance

The general mass balance for the dissolved oxygen in the liquid phase can be rearranged as:

$$\frac{dO_2}{dt} = k_L a \cdot \left(O_2^* - O_2\right) - q_{O_2}\left(O_2\right) \cdot X \qquad \text{(A.1)}$$

where dO_2/dt is the oxygen accumulation specific rate in the liquid phase, k_La is the volumetric oxygen mass transfer coefficient, X is the total biomass measured, O_2^* is the oxygen equilibrium concentration and $q_{O_2}\left(O_2\right)$ is the specific oxygen uptake rate, which depends on the dissolved oxygen concentration. The latter can be described as the product of two terms, the maximum specific oxygen uptake rate, $q_{O_2,\max}$, and a function of the dissolved oxygen, $f(O_2)$. The incorporation of this last term to Eq. (A.1), allowed describing heterogeneous mixing conditions in the bioreactor, which could account for the oxygen concentration gradients present in oenological fermentations. The choice of the $f(O_2)$ function for describing different hydrodynamic conditions was, therefore, based on its ability to reproduce empirical data. Under ideal mixing conditions, we found that $f(O_2)$

can be described by a sigmoid function, similar to the Hill equation (Villadsen et al., 2011).

$$f\,(\mathrm{O}_2) = \frac{\mathrm{O}_2^n}{\mathrm{O}_{2,\mathrm{crit}}^n + \mathrm{O}_2^n} \qquad \text{(A.2)}$$

where $O_{2,crit}$ and n are empirical model parameters. The former represents the dissolved oxygen level necessary to reach half of the consumption response; and the latter is an affinity parameter. Under non- agitated conditions, *i.e.* mechanical mixing was avoided, a different $f(O_2)$ function was chosen since the shape of the uptake kinetics changed. A linear, single parameter ($O_{2,s}$) function was sufficient to describe the observed oxygen consumption kinetics.

$$f\,(\mathrm{O}_2) = \frac{\mathrm{O}_2}{\mathrm{O}_{2,\mathrm{s}}} \qquad \text{(A.3)}$$

A.3.2 Oxygen solubility

To estimate the oxygen solubility in terms of the fermenting medium composition, an empirical log-additivity model was developed and calibrated with data taken from the literature (Schumpe et al., 1982; Rischbieter et al., 1996; Gros et al., 1999):

$$\log_{10}\left(\frac{H_{\mathrm{mix}}}{H_{\mathrm{w}}}\right) = \sum_j^m K_j(T)\cdot C_j \qquad \text{(A.4)}$$

where H_{mix} and H_w denote the Henry's constants in the solution and in pure water, respectively; C_j denotes the concentration of the compound j in the solution; and K_j is the Sechenov constant, which is slightly dependent on the temperature and is specific to the

solute and the gas (Kutsche et al., 1984). The compounds considered in this model are mainly sugars and alcohols. Rischbieter and Schumpe (1996) have demonstrated that the latter can be well represented by a linear function of the temperature. We found that a simple proportionality relation (A.5) was sufficient to fit the experimental data to the proposed model.

$$K_j(T) = \quad_j T \qquad \text{(A.5)}$$

where β_j is a model parameter estimated from experimental solubility data of solutions containing only the compound *j* for the specific gas and *T* is the temperature in Kelvin. The Henry's constant of oxygen in pure water can be calculated using the empirical equation proposed by Rettich (2000),

$$\ln\left(H_{\mathrm{w}}\right) = A + \frac{B}{T} + \frac{C}{T^2} \qquad \text{(A.6)}$$

where *A*, *B* and *C* are model parameters calculated from experimental data. Using Henry's law and Eqs. (A.4), (A.5) and (A.6), the dissolved oxygen concentration in equilibrium with the bulk gas phase is given by,

$$\mathrm{O}_2^* = \frac{p_{\mathrm{O}_2}}{H_{\mathrm{mix}}} \qquad \text{(A.7)}$$

where p_{O_2} is the oxygen partial pressure in the gas phase.

A.4 Materials and Methods

A.4.1 Yeast strain

The commercial *Saccharomyces cerevisiae* wine strain EC1118 Prise de Mousse (Lalvin, Zug, Switzerland) was used in these experiments. Yeasts were precultured in YPD medium at 28ºC in 125 mL Erlenmeyer flasks.

A.4.2 Culture media and fermentation conditions

Batch fermentations were carried out in a Bioflo IIc bioreactor (New Brunswick Scientific Co., Edison, N.J.) starting with 2.5 L of modified MS300 medium (Salmon and Barre 1998) containing (per liter): 120 g of glucose, 6 g of DL-malic acid, 6.32 g of citric acid monohydrate, 156 mg of $CaCl_2 \cdot 2\ H_2O$, 750 mg of KH_2PO_4, 500 mg of K_2SO_4, 250 mg of $MgSO_4 \cdot 7H_2O$, 200 mg of NaCl, 4 mg of $MnSO_4 \cdot H2O$, 7.2 mg of $ZnSO_4 \cdot 7H_2O$, 1 mg of $CuSO_4 \cdot 5H_2O$, 1 mg of KI, 0.4 mg of $CoCl_2 \cdot 6H_2O$, 1 mg of H_3BO_3, 1 mg of $NaMoO_4 \cdot 2H_2O$, 20 mg of myo-inositol, 2 mg of nicotinic acid, 1.5 mg of calcium pantothenate, 0.25 mg of thiamine hydrochloride, 0.003 mg of biotin, and 0.25 mg of pyridoxine hydrochloride. The ammoniacal nitrogen and amino acids concentration in the medium were the same used by Salmon and Barre (1998), except that we did not use proline. The initial nitrogen concentration for batch fermentations was 300 mg L^{-1}. The inoculation was done to obtain 10^6 cells mL^{-1}. The pH and temperature were maintained at 3.5 and 25ºC respectively, while the stirring speed was set to 300 rpm throughout the cultivation.

A.4.3 Analytical techniques

Periodic samples were taken to analyze biomass (dry cell weight per liter) and the concentration of main metabolites, following the method described in Varela et al. (2004).

A.4.4 Oxygen additions

During the fermentation course, pure oxygen (99.7% purity) additions of 0.3 L min^{-1} were carried out during 1 min approximately, with and without agitation after the addition. To study the agitation effect on the oxygen consumption kinetics, oxygen pulses without agitation were carried out during the exponential growth phase (X > 2.5 gDW L^{-1}). The additions were performed using a cylindrical pore diffuser with a pore mean diameter of approximate 20 µm at the bottom of the bioreactor. The oxygen pulse was stopped when dissolved oxygen reached 3 to 6 mg L^{-1}, oxygen levels that were reported to be beneficial for yeast performance (Sablayrolles and Barre, 1986).

A.4.5 Dissolved oxygen

The oxygen concentration was measured with a 3 LCD-trace Fibox v7 machine (PreSens®, Regensburg, Germany) that included temperature compensation. This optical sensor does not have the problems of the Clark's electrode, *e.g.* relatively long response times and oxygen consumption during the measurement (Fernández-Sánchez et al., 2007). Moreover, most of these electrodes have a response time close to the characteristic time for the mass transfer process, and the measured concentrations are therefore influenced by the dynamics of the measurement device (Villadsen et al., 2011). The oxygen kinetics were followed with two optical sensors PSt3 (PreSens®, Regensburg, Germany) placed inside

the reactor with ideal measurement ranges for dissolved oxygen between 0 to 45 mg L^{-1}; one measuring the dissolved oxygen within the liquid phase and the other the oxygen partial pressure inside the reactor headspace.

A.4.6 Oxygen solubility

Saturation experiments were performed with synthetic air (20% oxygen and 80% nitrogen from Indura, Santiago, Chile) and pure oxygen (99.7% purity also from Indura) using different test solutions in a 2.5-L agitated Bioflo IIc bioreactor and measured with the 3 LCD-trace Fibox v7 device. First, all dissolved gases were desorbed by nitrogen injection until oxygen concentrations lower than 40 µg L^{-1} were reached. Then, pure oxygen or synthetic air was injected until the liquid phase reaches saturation with oxygen. Equilibrium concentration was recorded when dissolved oxygen concentration variations were less than ±1%.

A.4.7 k_La measurements in synthetic solution

The estimation of the volumetric mass transfer coefficient in a model solution without biomass was performed using the conventional dynamic method described by Devatine et al. (2007). Measurements were carried out in a liquid medium that mimics the exponential growth phase (per liter): 80 g of glucose, 1.5 g of glycerol, 12.6 g of ethanol, 50 mg of nitrogen, 6.32 g of citric acid monohydrate, 6 g of DL-malic acid, 156 mg of $CaCl_2 \cdot 2\ H_2O$, 525 mg of KH_2PO_4, 350 mg of K_2SO_4, 160 mg of $MgSO_4 \cdot 7H_2O$, 140 mg of NaCl, 2.8 mg of $MnSO_4 \cdot H_2O$, 5 mg of $ZnSO_4 \cdot 7H_2O$, 0.7 mg of $CuSO_4 \cdot 5H_2O$, 0.7 mg of KI, 0.28 mg of $CoCl_2 \cdot 6H_2O$, 0.7 mg of H_3BO_3, 0.7 mg of $NaMoO_4 \cdot 2H_2O$. The influence of

dissolved carbon dioxide on the volumetric mass transfer coeficient was also assessed using this medium. Measurements were carried out in the synthetic medium without dissolved carbon dioxide and with carbon dioxide saturation concentrations of 1.2 g L^{-1} at 25°C.

A.4.8 Parameter fitting

The most common and reproducible method for measuring the OUR is the standard dynamic method (Garcia-Ochoa et al., 2010), which is only suitable for continuous aeration processes, but it is impracticable for wine fermentation. Instead, we propose a dynamic method for modeling the OUR and OTR during the addition of controlled oxygen pulses based on the absorption-desorption cycle shown in Figure A-1. First, the OUR model parameters ($q_{O_2,max}$, n and $O_{2,crit}$) and the oxygen stripping term (k_La_{strip}) are dynamically estimated from the desorption curve until the dissolved oxygen concentration is approx. 40 µg L^{-1}. The oxygen mass balance during the desorption stage is given by,

$$\frac{dO_2}{dt} = -k_L a_{strip} \cdot O_2 - q_{O_2}(O_2) \cdot X \qquad \text{(A.8)}$$

where k_La_{strip} corresponds to the volumetric oxygen mass transfer coefficient caused by the carbon dioxide bubbles naturally present during the fermentation. Then, the volumetric oxygen mass transfer coefficient (k_La) is estimated from the absorption curve using the oxygen uptake model parameters previously fitted and the oxygen solubility model, thus completing the cycle. In this case, Eq. (A.1) applies.

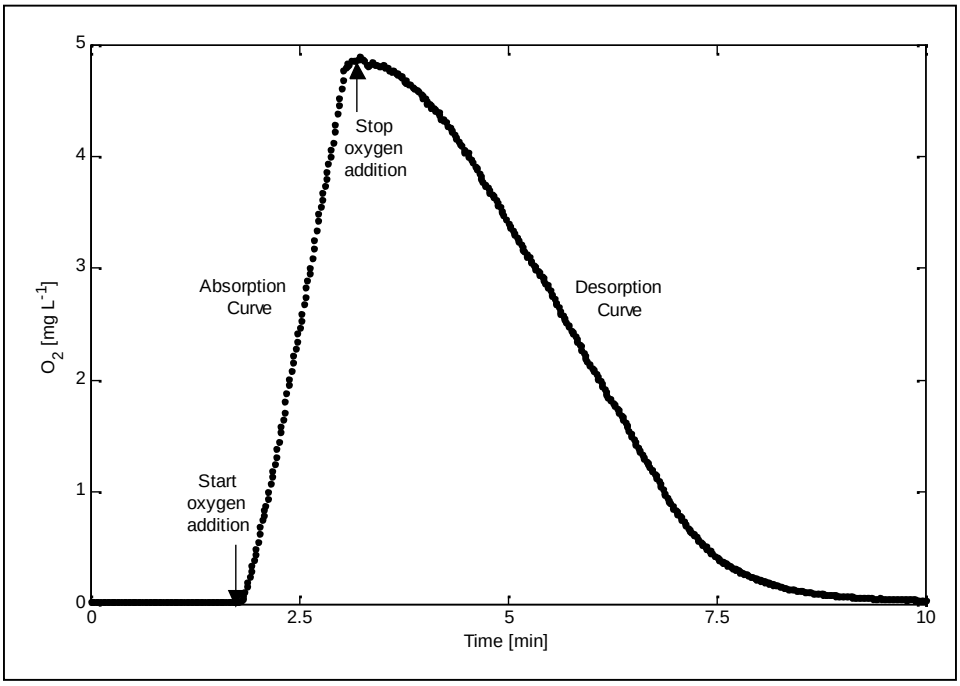

Figure A-1: A typical absorption-desorption cycle occurring during an oxygen impulse under oenological conditions

Model parameters were estimated in each stage by minimizing the sum of squared residual errors between predicted and experimental data,

$$\underset{\Theta}{\text{Min}} \sum_{k}^{N} \left(O_2^{\text{model}} - O_2^{\text{meas}} \right)^2 \qquad \text{(A.9)}$$

where Θ denotes the parameter space, O_2^{model} is the dissolved oxygen concentration predicted, O_2^{meas} is the dissolved oxygen concentration measured and *N* represents the number of measurements. This procedure was solved numerically using integration and non-linear optimization routines within MATLAB®. We found the local solver *fminsearch* to be effective for dynamic optimization of the oxygen mass balance model parameters and *nlinfit* for non- linear regression of the oxygen solubility model parameters. The function

ode113, a variable order Adams–Bashforth–Moulton solver, was employed for ODE integration.

A.4.9 Regression diagnostics

The procedures required to test the quality of the parameter estimation consider the calculation of the parameter sensitivity, parameter identifiability and parameter significance. These tests were performed as described by Sacher et al. (Sacher et al., 2011), except that in the case of the 95% confidence interval calculation, the MATLAB® functions *nparci* and *nlpredci* were applied. The analysis of the results of the regression diagnostics allowed us to postulate models with different number of parameters. To compare goodness-of-fit of these models, Akaike's Information Criterion (AIC) was employed (Bonate, 2011). The AIC is calculated as (Wang et al., 2011):

$$\mathrm{AIC} = N \ln\left(\frac{RSS}{N}\right) + 2\left(p+1\right) + \frac{2\left(p+1\right)(p+2)}{(N-p-2)} \qquad \text{(A.10)}$$

where *RSS* is the sum of the squared residuals and *p* is the number of parameters to fit. The model with the smallest AIC is the recommended choice (Bonate, 2011).

A.5 Results and discussion

A.5.1 Calibration of the oxygen solubility model

The substances considered in the model were those with the higher concentrations during the fermentation course, *i.e.* ethanol, glucose and fructose. The influence of organic acids on oxygen solubility was neglected, because of their relative low concentrations in wines (Castiñeira et al., 2002). Oxygen solubility data in pure water at different

temperatures was obtained from the work of Wilhelm et al. (Wilhelm et al., 1976), and then used to fit the parameters in Eq. (A.6). In the case of glucose and fructose, experimental results reported by Eya et al. (Eya et al., 1994) and Mishima et al. (Mishima et al., 1996) were used, respectively. The situation is more complex in the case of oxygen solubility in hydroalcoholic solutions. Several authors (Kutsche et al., 1984; Luhring and Schumpe, 1989; Cargill R.W., 1993) have shown that, at low ethanol concentrations, and depending upon the temperature, an increase or decrease of the oxygen solubility was observed (Chiciuc et al., 2010). For parameter calibration, we used the results obtained by Cargill (1993) for hydroalcoholic solutions, where a decrease of oxygen solubility up to 0.15 ethanol mole fraction was reported. The fitted parameters are shown in Table A-1 with their corresponding 95% confidence intervals.

Table A-1: Fitted parameters of the oxygen solubility model for temperatures ranging between 15 and 37°C

Model	Parameter	Value
Henry's constant in pure water	A	-5.9 ± 1.2
$\ln(H_w) = A + \frac{B}{T} + \frac{C}{T^2}$	B	$3.0\times10^{3} \pm 7.1\times10^{2}$
A [-], B [K], C [K^2]	C	$-6.9\times10^{5} \pm 1.0\times10^{5}$
Sechenov constant	β_{glu}	$2.3\times10^{-6} \pm 1.7\times10^{-7}$
$K_j(T) = {}_jT$	β_{fru}	$2.2\times10^{-6} \pm 1.5\times10^{-7}$
β_j [L g^{-1} K^{-1}]	β_{etOH}	$1.2\times10^{-6} \pm 8.2\times10^{-8}$

Model predictions agreed with validation experiments performed at 25°C with a mean relative error of 2.1% (Table A-2). Larger deviations in validation experiments are observed in saturation experiments performed with air, although the relative error is low (less than 3%). This result can be explained because the model was calibrated using only solubility data with pure oxygen. Another possible source of error in the determination of oxygen solubility is that the oxygen partial pressure was not corrected by the water vapor pressure at 25°C, though its value is very low (approx. 0.03 atm) under the conditions considered. We suspect that this term in our case can be neglected, since the experimental set up for determining oxygen saturation concentration used a continuous flow of pure oxygen or synthetic air equilibrated at 1 atm. In fact, comparison with more complicated methods already published in the literature for measuring oxygen solubility in artificial media (Rasmussen, 2003) show agreement with our solubility data. Finally, given that the experimental measurement error of the data used for parameter fitting and the precision of the validation experiments were around ±1.5% and ±1%, respectively, the proposed model

showed satisfactory results which fell within the measurement's experimental error. These results also agreed with the results obtained using the solubility model proposed by Rasmussen et al. (2003) for different artificial media.

Table A-2: Validation of the oxygen solubility model at 25°C

Medium	O^*_2 with air in mg L^{-1}			O^*_2 with pure oxygen in mg L^{-1}		
	Exp.	Model	Rel. error (%)	Exp.	Model	Rel. error (%)
Distilled water	8.0	7.9	1.3	38.7	39.2	1.3
12% v/v ethanol	7.1	7.3	2.8	36.8	36.4	1.1
8% v/v ethanol, 55 g L^{-1} fructose, 25 g L^{-1} glucose	6.8	6.6	2.9	33.9	33.0	2.7
Fermentation medium[a]	7.0	6.8	2.9	34.8	34.2	1.7

[a] Medium composition was the same used for k_La measurements in synthetic solution, as described in Materials and Methods

A.5.2 Oxygen uptake rate model calibration under perfect mixing conditions

To determine the optimal OUR model, we first performed calibrations considering the four model parameters for each pulse addition experiment. Parameter significance tests showed that during the stripping stage, k_La_{strip} lacked statistical significance; hence, it could be discarded from the model. The latter was experimentally verified, by showing that almost no oxygen could be measured in the headspace after stopping oxygen addition (not shown). Furthermore, oxygen balance showed that less than 3.5% of the injected oxygen was lost by CO_2 stripping.

The model was then calibrated with three parameters: n, $q_{O_2,max}$ and $O_{2,crit}$. This reduced parameter model featured smaller confidence intervals and increased the significance of the parameter set; however, some identifiability problems were

encountered, in particular in the case of parameters $q_{O_2,max}$ and n. The estimated correlation coefficient, κ, for these parameters was 0.98 for the experimental time. On the other hand, the sensitivity analysis showed that the $O_{2,crit}$ parameter presents a relatively low sensitivity (Fig. A-2). In addition, fitted values ranged between 0.18 and 0.45 mg L^{-1}. Hence, to solve this lack of identifiability, $O_{2,crit}$ was arbitrarily set to 0.3 mg L^{-1}. Normally, one can fix those parameters whose values are given in the literature or can be obtained by independent experiments (Ingalls, 2003; Degenring, 2004; Schwacke and Voit, 2005; Zak et al., 2005); however, this was not our case, since there are no related data about this parameter. Nonetheless, the employed value agrees with the literature, since the saturation constant of oxygen for *S. cerevisiae*, K_o, is in the range of 1 – 10 µM, which corresponds approximately to oxygen concentrations of 0.03 – 0.33 mg L^{-1} at 25°C and 1 atm of air (Villadsen et al., 2011).

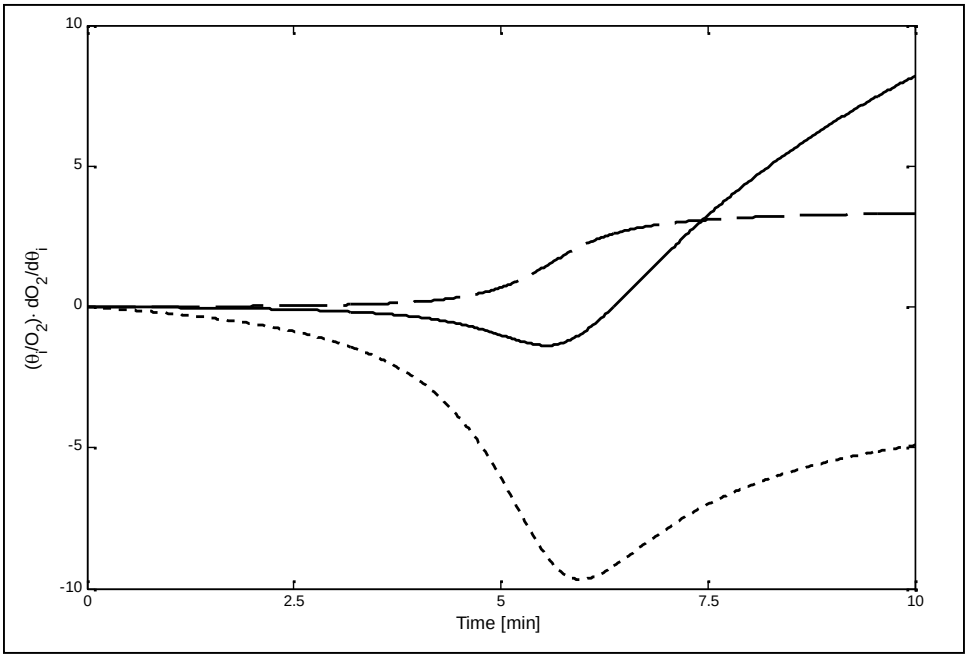

Figure A-2: Time-dependent normalized sensitivities of the OUR parameters model during the experiment. The solid line corresponds to the sensitivity of the parameter *n*, while the dashed and dotted lines represent the sensitivities of the $O_{2,crit}$ and $q_{O_2,max}$ parameters, respectively

The reduced parameter space improved the parameter significance and solved the lack of determinability. Model 3 showed the smallest AIC (Table A-3), confirming that this was the best choice.

Table A-3: Comparison of the different models

Model	Estimated parameters	Significant parameters	Correlated parameters	AIC
1	k_La_{strip}, n, $q_{O_2,max}$, $O_{2,crit}$	n, $q_{O_2,max}$, $O_{2,crit}$	k_La_{strip}, $q_{O_2,max}$	-828
2	n, $q_{O_2,max}$, $O_{2,crit}$	n, $q_{O_2,max}$, $O_{2,crit}$	n, $q_{O_2,max}$	-845
3	n, $q_{O_2,max}$	n, $q_{O_2,max}$	-	-867

A.5.3 Comparison of experimental results and model predictions

Oxygen consumption kinetics, as well as the two parameter OUR model fitting, are illustrated in Figure A-3. As previously mentioned, the decrease in the dissolved oxygen concentration corresponds to biological consumption of oxygen by the yeast. Oxygen consumption under anaerobic conditions is explained mainly by the oxygen utilization in sterols and unsaturated fatty acids pathways and other cellular processes that still are not well characterized (Rosenfeld et al., 2002).

The proposed two parameter OUR model fits the data well, with mean relative differences with the experimental data of 2%. As expected, oxygen consumption rates strongly depend on the biomass concentration (Figure A-3). Under perfect mixing conditions, the first part of the oxygen consumption kinetics can be represented by a straight line, as in aerobic processes, at least until dissolved oxygen concentration reaches 0.6 – 0.8 mg L^{-1} ($\approx 2 \cdot O_{2,crit}$). When the dissolved oxygen falls below this critical level, the oxygen consumption rate decreased significantly, until a plateau was reached. This behavior is mainly described by the $f(O_2)$ function for low oxygen concentrations and agrees with Doran (1995), who reports a critical level for dissolved oxygen concentration beyond which the specific oxygen consumption rate (q_{O_2}) by a microorganism reaches a maximum constant level $q_{O_2,max}$. Below this level, q_{O_2} is largely influenced by the dissolved oxygen concentration, falling in an oxygen-limiting region (Fig. A-4a).

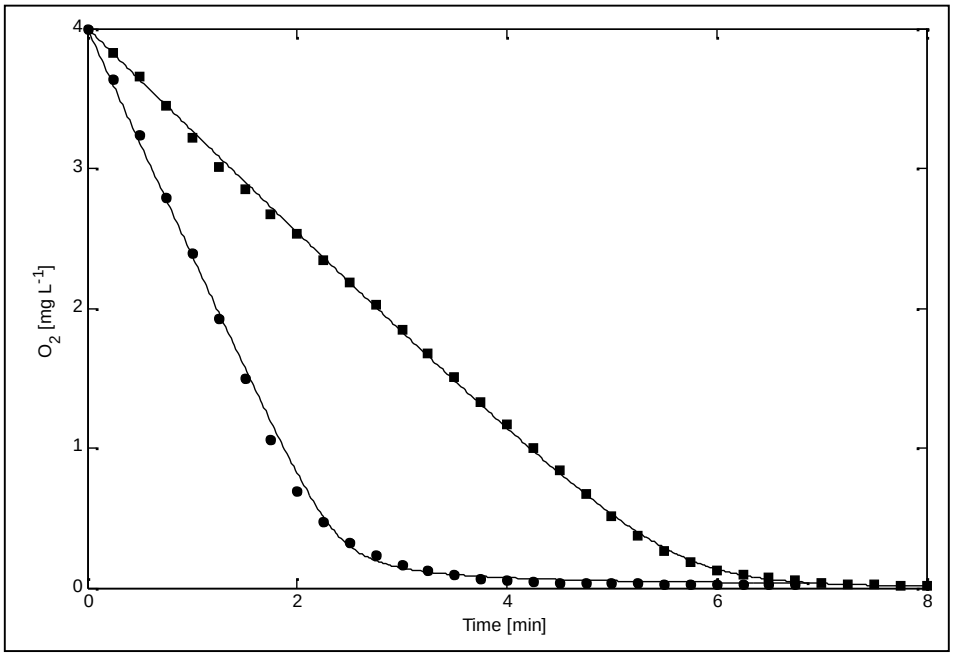

Figure A-3: Oxygen uptake rate model for different biomass concentrations during oenological fermentations. The black squares and circles correspond to experimental measurements performed with biomass concentrations of 2.9 and 5.0 gDW L^{-1}, respectively. Solid lines represent model predictions. The fitted parameters were $O_{2,crit}$ = 0.3 mg L^{-1}, $q_{O_2,max}$ =16.2 mg O_2 gDW^{-1} h^{-1} and n = 1.5 in the case of X = 2.9 gDW L^{-1}, while in the case of X = 5.0 gDW L^{-1} the fitted parameters were $O_{2,crit}$ = 0.3 mg L^{-1}, $q_{O_2,max}$ =19.4 mg O_2 gDW^{-1} h^{-1} and n = 2.3

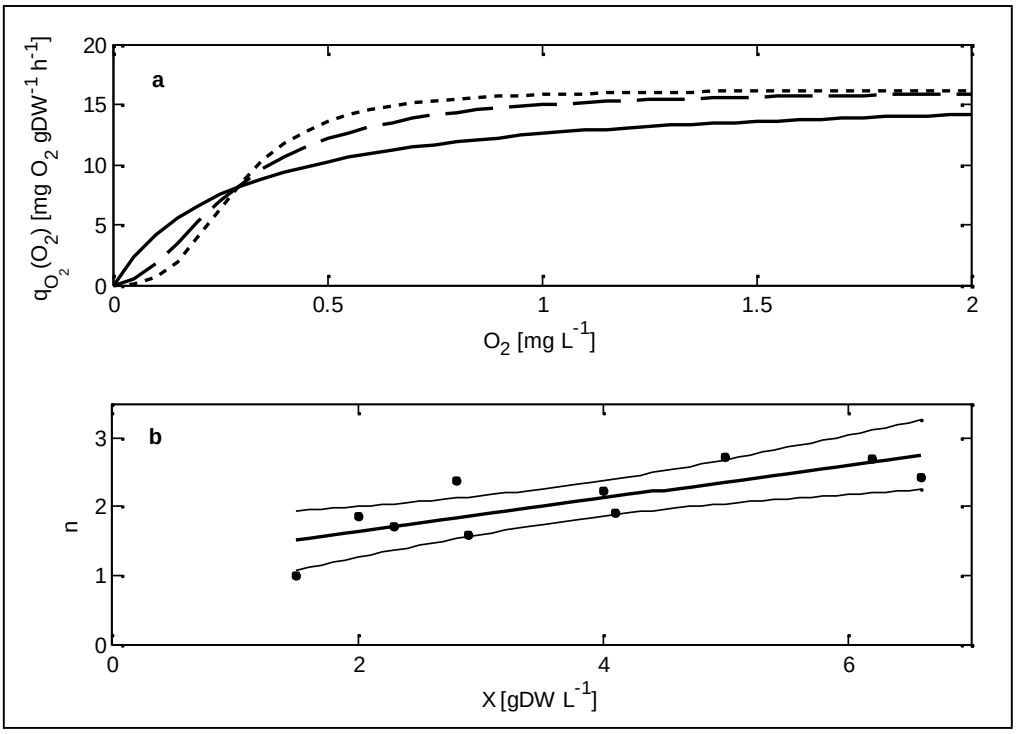

Figure A-4: Specific oxygen consumption kinetics by *Saccharomyces cerevisiae* and increase of the parameter *n* with the biomass concentration. **a**: Behavior for different *n* values (solid line $n = 1$, dashed line $n = 2$ and dotted line $n = 3$). **b**: Fitting of *n* for different biomass concentrations (the higher the biomass concentration the larger the values of *n*). The thicker line represents a linear regression between both variables, while the thinner lines denote the 95% confidence interval of the trend of the fitted values (black dots)

According to the proposed model, the specific oxygen uptake rate depends not only on $O_{2,crit}$ but also on *n*. When the value of *n* increases, the maximum specific oxygen uptake rate is reached faster in the oxygen-limiting region ($O_2 < 2 \cdot O_{2,crit}$) (Fig. A-4a).

Considering that the higher the biomass concentration the larger the values of *n* (Fig. A-4b), it appeared that the culture becomes more sensitive to low oxygen levels at higher biomass concentrations. The latter could contribute also to explain why oxygen additions performed at the end of the cell growth phase are key to completing the fermentation (Sablayrolles et al., 1996).

OUR depends on biomass content and the specific oxygen uptake rate. Model calibrations show that the specific oxygen uptake rate varies during the fermentation (Fig. A-5). Maximum specific rates of 16.2 to 19.8 mg O_2 gDW^{-1} h^{-1} were observed during the exponential growth phase, *i.e.* for $X \approx 4.0$ gDW L^{-1}, while the oxygen consumption rate decreased at the end of the growth phase (11.8 to 14.4 mg O_2 gDW^{-1} h^{-1}). This trend is similar to the one observed for microorganisms growing in aerobic cultures; however, the computed values for *S. cerevisiae* wine strain are comparatively lower than those of similar aerobic microorganisms (Garcia-Ochoa et al., 2010).

Maximum OUR values were reached at the end of the growth phase, as already reported by Sablayrolles (Sablayrolles et al., 1996). However, OUR values estimated in the present research are considerably higher than the values reported in the literature. Maximum OUR values reached up to 108 mg O_2 L^{-1} h^{-1}, which is approx. six times greater than the values reported in previous articles (Sablayrolles and Barre, 1986; Sablayrolles et al., 1996). This difference can be explained by the different methods employed for measuring the oxygen uptake. Previous works employed oxygen electrodes for measuring the oxygen uptake. These types of sensors require a continuous flow of oxygen through a

prepared culture sample because they consume oxygen during the measurement. For this reason, they cannot be used to measure the consumption directly in the bioreactor. On the contrary, optical sensors such as those employed in this paper allow measuring the dissolved oxygen concentration *in situ* under more realistic conditions and without interfering with the oxygen uptake because they do not consume oxygen.

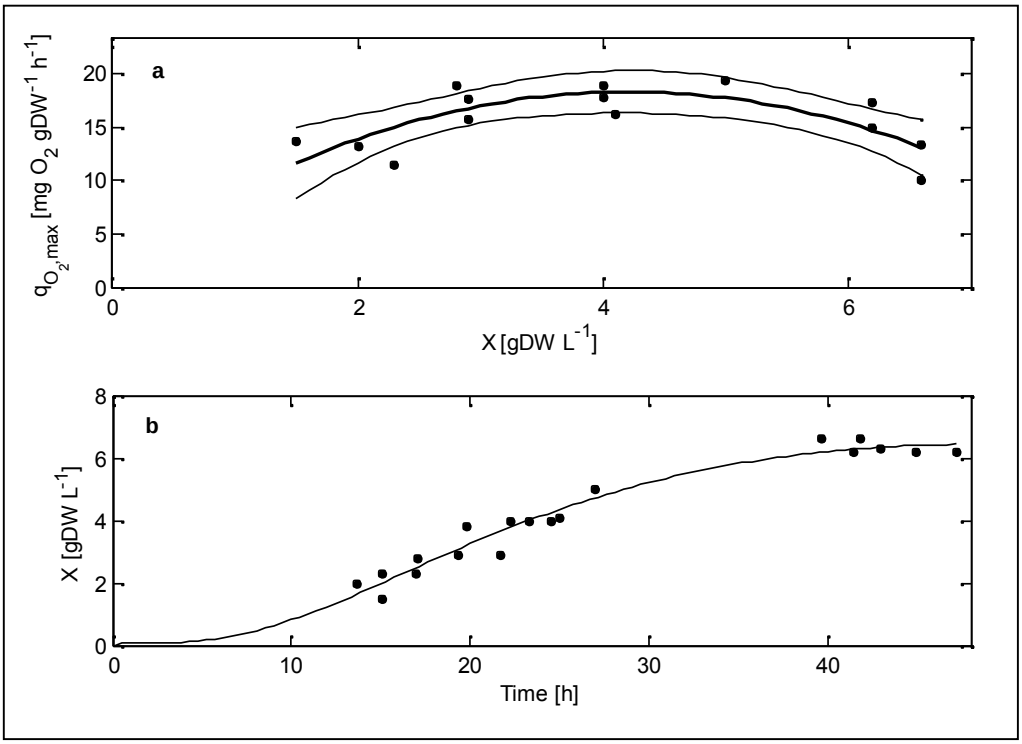

Figure A-5: Specific oxygen uptake rate optimization and biomass growth. **a**: Evolution of the specific oxygen uptake rate with the biomass concentration. The thicker line represents a quadratic regression between both variables, while the thinner lines denote the 95% confidence interval of the trend of the fitted values (black dots). **b**: Biomass concentration along the fermentation. Black dots represent

biomass concentration measurements and the solid line represents the fermentation course

A.5.4 Oxygen uptake rate model calibration under non- agitated conditions

In contrast with the model developed for agitated conditions, the model proposed for describing oxygen uptake kinetics under non- agitated conditions lacked structural identifiability, since the $q_{O_2,max}$ and $O_{2,s}$ parameters are correlated (κ = 1.0). Considering that the $q_{O_2,max}$ parameter changes continuously during the fermentation depending on the growth phase, and that we do not have reliable values for the $O_{2,s}$ parameter, we decided to estimate them together as one single key parameter, $q_{O_2,max}/O_{2,s}$. As expected, this modification solved the model's identifiability problem.

A.5.5 Influence of agitation conditions upon the oxygen uptake response time

Figure A-6 shows the different model fittings obtained with and without agitation for the same biomass concentration. Satisfactory fittings were obtained in the case of no agitation, confirming the suitability of the $f(O_2) = O_2/O_{2,s}$ function chosen. Mean relative differences with the experimental data were around 5%. As illustrated in Figure A-6, the oxygen response curve in non- agitated conditions is different from that in agitated conditions, both in shape and time of decay.

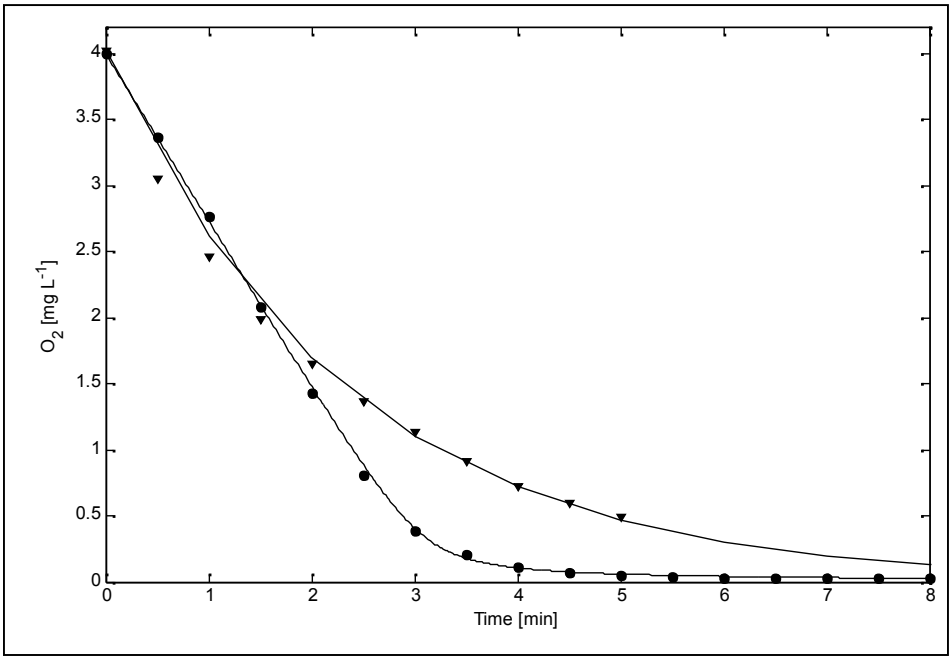

Figure A-6: Comparison of different oxygen consumption dynamics for different hydrodynamic conditions. The biomass concentration in both cases was 4.0 g DW L^{-1}. For both experiments, the pH and temperature were maintained at 3.5 and 25ºC, respectively. The black circles correspond to the oxygen uptake measurements at a stirring speed of 300 rpm, while the black triangles denote measurements without agitation. Solid lines represent model predictions. The fitted parameters were $O_{2,crit}$ = 0.3 mg L^{-1}, $q_{O_2,max}$ =19 mg O_2 gDW^{-1} h^{-1} and n = 2.2 in the case with agitation, while in the case without agitation the fitted parameter was $q_{O_2,max}/O_{2,s}$ = 0.4 L gDW^{-1} h^{-1}

The influence of the mixing conditions on the oxygen uptake response time was assessed by comparing the response time for both kinetics (Stephanopoulos, 1984). The response time, $t_{95\%}$, is the time needed to reach the ±5% interval of its final value and to

stay there. Using the respective expressions for the oxygen uptake under mixing and non-mixing cultivation, the response times in both conditions can be calculated as,

$$t_{95\%}^{\text{mixing}} = \frac{0.95 \cdot \mathrm{O}_2(t=0)}{q_{\mathrm{O}_2} \cdot X} \qquad \text{(A.11)}$$

$$t_{95\%}^{\text{no mixing}} = \frac{\ln(20) \cdot \mathrm{O}_{2,s}}{q_{\mathrm{O}_2} \cdot X} \qquad \text{(A.12)}$$

The estimated constants were statistically different - *t*-test for unequal variances at 95% confidence level gave a *p*-value of 6.4×10^{-3}, reaching 3.0 ± 0.8 min and 7.9 ± 2.2 min for the agitated and non- agitated conditions, respectively. Hence, the hydrodynamic condition significantly affects the response time of the oxygen uptake kinetics. When the culture is non- agitated, the response time increases by a factor of 1.5 to 2.6, confirming results reported in the literature of the importance of mixing during mass transfer in biological uptake processes (Gagnon et al., 1998). Caşcaval et al. (2011) showed that a unique distribution of oxygen transfer rates occurred within a stirred bioreactor, depending on the geometrical and operational characteristics of the vessel, medium composition and type and concentration of the microorganism, among other factors. In the case of *S. cerevisiae* broths, it was observed that the tendency of yeast cells to settle plays a key role in the oxygen transfer rates distribution. This result can help to understand why the oxygen uptake response is different. Without agitation, yeast cells tend to accumulate at the bottom, slowing down the measured response at the location of the probe and changing the slope of the oxygen uptake curve.

Finally, oxygen partial pressure measurements at the reactor headspace found no significant differences in the oxygen lost by stripping between agitated and non- agitated cultures (mean relative difference less than 1%).

A.5.6 Oxygen mass transfer under oenological conditions

The developed models for oxygen solubility and OUR were employed to properly estimate the k_La coefficient during the absorption stage (Figure A-7a). The estimated k_La values increased from 5.14 to 13.43 h^{-1}, when OUR increased from 20 to 108 mg O_2 L^{-1} h^{-1}. Similar trends have been reported for aerobic cultures (Vashitz et al., 1989; Calik et al., 1997; Çalik et al., 2004; Djelal et al., 2006) also. Moreover, it was found that the k_La and the OUR can be linearly correlated. However, k_La values obtained when biomass was present are lower than the k_La estimated in a synthetic solution saturated with 1.2 g L^{-1} of CO_2 without biomass (16.7 ± 0.5 h^{-1}). Thus, the oxygen transfer observed with biomass present is slower than without biomass (Fig. A-7b). The latter could result from compositional changes of the culture, as well as from an increase in the broth's viscosity during the fermentation course. The increased medium viscosity increases the liquid film resistance to mass transport, negatively affecting the volumetric mass transfer coefficient (Garcia-Ochoa et al., 2010; Caşcaval et al., 2011). Hence, the positive effect of the OUR on the OTR is not large enough to compensate the increased mass transport resistance of the medium during the absorption of oxygen under oenological conditions.

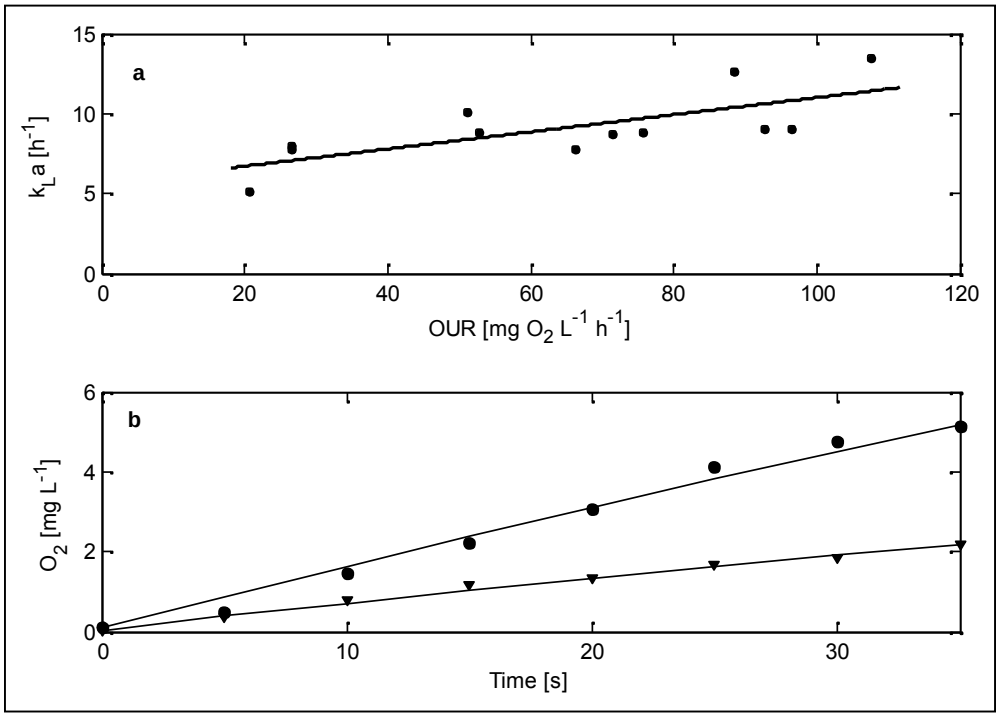

Figure A-7: Oxygen mass transfer under oenological conditions. **a**: Correlation between the oxygen uptake rate and the estimated k_La. The thicker line represents a linear regression between both variables (R = 0.72). **b**: Comparison of different absorption curves in microbial culture (black triangles, k_La = 8.2 h^{-1}) and in sterile medium (black dots, k_La = 16.6 h^{-1}). Solid lines denote the model predictions. The biomass concentration was 2.9 g DW L^{-1} in the case of the medium with oxygen consuming yeasts. The estimated oxygen solubilities were 34.2 mg L^{-1} in the sterile medium and 33.5 mg L^{-1} in the microbial culture

A.5.7 Influence of the dissolved carbon dioxide upon the mass transfer coefficient

The dissolved carbon dioxide effect upon the estimated k_La in synthetic fermentation media was also assessed. Estimations of the k_La were carried using the conventional dynamic method (Devatine et al., 2007). The k_La value obtained in CO_2 free media was 47.2 ± 7.2 h^{-1}, three times higher than the value obtained in the same solution saturated with 1.2 g L^{-1} carbon dioxide. Similar results were reported by Devatine et al. (2007) for wines, thus confirming the negative influence of the carbon dioxide on the estimated k_La value in oenological fermentations.

A.6 Conclusions

The experimental methodology employed in this research allowed us to develop a model of the oxygen kinetics under similar conditions to those encountered in oenological fermentations on an industrial scale. The model accurately describes the oxygen kinetics observed during discrete oxygen additions under oenological conditions on a laboratory scale. We showed that the specific oxygen uptake rate of the *S. cerevisiae* wine strain strongly depends on the growth phase and that the oxygen mass transfer coefficient is modified by the biological uptake. Estimated k_La values increased from 5.14 to 13.43 h^{-1}, when OUR increased from 20 to 108 mg O_2 L^{-1} h^{-1}. However, our results suggest that the positive effect of the biological uptake on the oxygen mass transfer coefficient is not large enough to compensate the increased mass transport resistance of the medium due to compositional changes of the culture and the increased viscosity of the broth. The present model showed that agitation conditions have a significant effect on both the oxygen

consumption response time and the shape of the response curve. Finally, experimental and model results confirmed the negative effect of high levels of carbon dioxide upon the mass transfer coefficient, although oxygen stripping due to CO_2 bubbles is negligible during uptake.

APPENDIX B: IMPACT OF CARBON DIOXIDE INJECTION ON OXYGEN DISSOLUTION RATE DURING OXYGEN PULSE ADDITIONS IN A BUBBLE COLUMN

B.1 Abstract

Oxygen additions are common practice during oenological fermentations. Since oxygen dissolution under winemaking conditions is not completely understood, these additions are performed empirically. In particular, the influence of carbon dioxide produced by yeast cells on the oxygen dissolution rate remains unclear. In this paper, we describe an oxygen mass balance model that consists of two partial differential equations. The model reproduces the observed dissolved oxygen evolution at different locations in a laboratory scale carbon dioxide bubbling column during oxygen pulse additions. We found that carbon dioxide injection enhanced the volumetric mass transfer coefficient, but simultaneously decreased the oxygen solubility in the liquid phase. Overall, carbon dioxide injections reduce almost 60% the oxygen dissolution rate. The model developed here will help optimizing oxygen addition systems for oenological fermentations.

B.2 Introduction

Wine fermentation is mostly anaerobic. However, discrete oxygen additions are commonplace in most wineries as they allow increasing fermentation rates, contribute to the aromatic diversity, enhance color stability and favor palate development of the wines (Fornairon-Bonnefond et al., 2002; Salmon, 2006; Pérez-Magariño et al., 2007). Yeast cells require low oxygen doses - between 5 to 7.5 mg O_2 L^{-1} - to reduce the risk of sluggish fermentations (Sablayrolles and Barre, 1986; Rosenfeld et al., 2004). The timing of the oxygen addition is also important. Sablayrolles (1996) reported that the optimal moment for the latter is at the end of the growth phase, when carbon dioxide production is at his highest. Reported data show that oxygen enhances cell viability by promoting the synthesis of sterols and unsaturated fatty acids that ensure the integrity of the plasma membrane, especially at the final stages of the fermentation (Blayteron, L. and Sablayrolles, 2001). Nevertheless, oxygen could also be detrimental when added at too high concentrations, resulting in wine oxidation, color degradation and off-flavors synthesis (Adoua et al., 2010). Thus, understanding oxygen dissolution under conditions resembling oenological fermentation is critical to properly manage its addition.

Current oxygen additions are commonly carried out heuristically. The usual ways to incorporate O_2 into the industrial fermenting must are through pump-over or rack and return operations. In pump-overs, the fermenting must is pumped from the bottom of the tank and splashed over the skins/seeds cap that forms during fermentation; while for the rack and return technique, the fermenting must is racked into an empty tank, thus keeping

the grape solids separated from the fermenting must for a short period (most commonly for two to four hours), after which, the fermenting must is returned over the pomace in the starting tank (Boulton et al., 1996). Both techniques lack reproducibility in terms of oxygen incorporation and are difficult to study. However, there is an additional system to add small controlled amounts of oxygen to wine that consists in bubbling oxygen through spargers. This system is specially used during wine ageing in a process called micro-oxygenation, although it has been successfully implemented in laboratory and pilot scale fermentations, where the sparger is installed in the vessel or in a wine circulation loop (Sablayrolles et al. 1996; Blateyron et al., 1998; Silva and Lambri, 2006) Recently, Adoua et al. (2010) has developed a complex model based on Computational Fluid Dynamics (CFD) for simulating the oxygen mass transfer during wine micro-oxygenation (after fermentation) at industrial scale. Nevertheless, there are no reported models and specific experimental systems for studying the evolution of dissolved oxygen gradients in the fermenting must under oenological conditions after oxygen additions. Considering the high carbon dioxide production rates observed during the exponential phase of fermentation – between 0.9 and 1.2 g L^{-1} h^{-1}, (Casalta et al., 2010) - and the small amounts of oxygen added, around 60 mg O_2 L^{-1} h^{-1} (Sablayrolles et al. 1996), it can be argued that gaseous CO_2 plays a key role on the efficiency of oxygen dissolution during the addition. Therefore, to understand the oxygen dissolution phenomenon, we designed a bubble column system that allowed us to quantify and model oxygen pulse additions with simultaneous CO_2 injections under controlled conditions, simulating natural yeast CO_2 production during oenological fermentations.

The oxygen dissolution rate depends on both thermodynamics and mass transfer. On one hand, thermodynamics defines the oxygen equilibrium concentration under a given condition, which is involved in the evaluation of the transfer potential. On the other hand, the oxygen mass transfer determines the rate upon the equilibrium is reached, and depends on the volumetric mass transfer coefficient, k_La, and the hydrodynamic behavior. Hence, when modeling the oxygen dissolution rate, both terms must be properly estimated.

Several factors, such as temperature, oxygen partial pressure in the gas phase, pH and composition of the fermenting must or wine influence oxygen equilibrium (Singleton, 1987; Saa et al., 2012). The detrimental effect of dissolved carbon dioxide on oxygen equilibrium, *i.e.* its desorption into oxygen bubbles and the resulting decrease of oxygen partial pressure in the bubble stream, has also been reported (Devatine et al., 2007; Devatine and Mietton-Peuchot, 2009; Chiciuc et al., 2010). In contrast, there are no systematic studies on the volumetric mass transfer coefficient estimations under conditions resembling oenological fermentations, *e.g.* no mechanical mixing and high carbon dioxide production rates, critical to quantify more precisely oxygen dissolution in real musts. The volumetric mass transfer coefficient is affected by several factors, *e.g.* oxygen gas flow-rate, temperature, rheological characteristics of the medium and system's turbulence (Garcia-Ochoa and Gomez, 2009; Chiciuc et al., 2010). The latter is also associated with the hydrodynamic behavior which, in the case of bubble columns, is mainly influenced by the bubbles produced by the gas injection (Villadsen et al., 2011).

In this work, we developed an oxygen mass balance model able to reproduce the evolution of dissolved oxygen profiles observed in a laboratory scale bubble column during pulse additions with continuous carbon dioxide injection. The model describes both, the dissolved oxygen in the liquid and gas phase profiles by including empirical liquid recirculation and mixing correlations.

B.3 Modeling

The resulting dynamic oxygen mass balance model describes the response of oxygen dissolution in the liquid phase and oxygen depletion in the gas phase when a pulse is applied with simultaneous carbon dioxide injection. The main model assumptions are:

- Liquid velocity is considered only in the axial direction, *z*, and only depends on the radial position, *r*.
- Gas holdup is considered constant (Cachaza et al., 2008).
- Liquid film resistance around bubbles controls the overall mass transfer rate (Garcia-Ochoa and Gomez, 2009).
- Gas plug flow is assumed (Cachaza et al., 2008; Gourich et al., 2008).
- Radial dispersion term in the liquid phase can be neglected under the studied conditions (Rubio et al., 2004)
- Axial dispersion in the gas phase can be neglected because of its relatively low value when compared to D_z (Gourich et al., 2008)
- Axial evolution of pressure due to gravity can be neglected because of the relatively low height of the column (Rubio et al., 1999)

B.3.1 Oxygen mass balance model

The general oxygen mass balance for the dissolved oxygen concentration in the gas phase is given by (Cachaza et al., 2008; Gourich et al., 2008):

$$\frac{\partial C_G}{\partial t} = -\frac{k_L a}{\varepsilon_G}\left(C_G - m \cdot C_L\right) - \frac{U_G}{\varepsilon_G}\frac{\partial C_G}{\partial z} \qquad \text{(B.1)}$$

where $\partial C_G / \partial t$ is the oxygen dissolution rate in the gas phase; C_L represents the dissolved oxygen concentration; C_G denotes the oxygen concentration in the gas phase; k_La is the volumetric oxygen mass transfer coefficient; ε_G represents the average gas phase holdup; U_G is the superficial gas velocity and m is a dimensionless partition constant. This partition constant can be defined as $m = H/\left(R_{O_2} T\right)$, where H corresponds to the oxygen Henry's constant in water at 20 °C, T denotes the absolute temperature and R_{O_2} is the oxygen gas constant. On the other hand, the dynamic oxygen mass balance in the liquid phase can be obtained employing the expression proposed by Gupta et al. (2001) and the above mentioned model assumptions.

$$\frac{\partial C_L}{\partial t} = \frac{k_L a}{1-\varepsilon_G}\left(\frac{C_G}{m} - C_L\right) - u_L(r)\frac{\partial C_L}{\partial z} + D_z \frac{\partial^2 C_L}{\partial z^2} \qquad \text{(B.2)}$$

Where $\partial C_L / \partial t$ is the oxygen dissolution rate in the liquid; $u_L(r)$ denotes the liquid velocity profile and D_z denotes the axial dispersion coefficient. Equations (B.1) and (B.2) can be solved using such initial conditions that dissolved oxygen concentration at the beginning of the pulse (t = 0) is 0.5 mg L^{-1} and that the gas phase is depleted of oxygen,

$$C_{\mathrm{L}}(z, t=0) = 0.5 \text{ mg L}^{-1} \tag{B.3}$$

$$C_{\mathrm{G}}(z, t=0) = 0 \tag{B.4}$$

Boundary conditions, on the other hand, are those given by (Gourich et al., 2008),

$$\left.\frac{\partial C_{\mathrm{L}}}{\partial z}\right|_{z=0} = 0 \tag{B.5}$$

$$\left.\frac{\partial C_{\mathrm{L}}}{\partial z}\right|_{z=H_L/(1-\varepsilon_{\mathrm{G}})} = 0 \tag{B.6}$$

$$C_{\mathrm{G}}(z=0, t) = C_{\mathrm{G},0} \tag{B.7}$$

where $C_{\mathrm{G},0}$ represents the oxygen concentration in the gas phase at the inlet. The structure of the model allows solving independently Eq. (B.1) and (B.2) for each radius of the column, thus generating the entire dissolved oxygen profile during the addition as function of (*t*, *z*, *r*). This approach proved to be useful to model the dissolved oxygen profile in the presence of carbon dioxide bubbling as mentioned below.

B.3.2 Hydrodynamics

The liquid velocity profile produced during gas additions is extensively described in the literature. In this operation, liquid rises with the bubbles in the central portion of the column and flows downward in the outer annular section (Garcia-Calvo and Letón, 1994; Tobajas and Garcia-Calvo, 1996). There are several correlations that describe this behavior. One of the most successful expressions in reproducing experimental data is the one proposed by Wu and Al-Dahhan (2001),

$$\frac{u_L(r)}{u_{L0}} = 1 - 2.65 \cdot n^{0.44} \cdot c \cdot \left(\frac{r}{R}\right)^{2.65 \cdot n^{0.44} \cdot c} \tag{B.8}$$

where $u_L(r)$ represents the liquid recirculation profile, u_{L0} denotes the axial liquid velocity in the center of the column, R is the column radius and n and c are empirical model parameters. These model parameters were determined previously by Wu et al. (2001) for radial gas holdup profiles in bubble columns using the following expressions,

$$n = 2.188 \cdot 10^{3} \cdot \mathrm{Re}_G^{-0.598} \cdot \mathrm{Fr}_G^{0.146} \cdot \mathrm{Mo}_L^{-0.004} \tag{B.9}$$

$$c = 4.32 \cdot 10^{-2} \cdot \mathrm{Re}_G^{0.2492} \tag{B.10}$$

where Re_L represents the gas Reynolds number, Fr_G is the gas Froude number and Mo_L denotes the liquid Morton number. These dimensionless numbers are calculated by,

$$\mathrm{Re}_G = \frac{D_c U_G (°_L - °_G)}{«_L} \tag{B.11}$$

$$\mathrm{Fr}_G = \frac{U_G^2}{g D_c} \tag{B.12}$$

$$\mathrm{Mo}_L = \frac{g«_L^4}{(°_L - °_G)¥_L^3} \tag{B.13}$$

As mentioned earlier, u_{L0} represents the axial liquid velocity in the center of the bubble column and can be estimated employing the following expression (Ulbrecht et al., 1985),

$$u_{L0} = \frac{200 \cdot ¦_L}{D_c}\left[\left(\frac{U_G D_c}{¦_L}\right) \cdot \left(\frac{U_G^2}{g D_c}\right)^{-1/4}\right]^{0.92} \tag{B.14}$$

For the control case - without carbon dioxide injection - the liquid recirculation profile is calculated applying Eqs. (B.8) and (B.14) using the oxygen superficial velocity. However, when carbon dioxide injection is performed, the liquid velocity profile changes because of the distributed addition of this gas in the column. As a result, the liquid velocity rises and the profile flattens (Mudde et al., 2009). In order to reproduce this effect, the following expression was used to estimate the liquid recirculation profile,

$$u_{\mathrm{L}}(r) = u_{\mathrm{L},\mathrm{O}_2}(r) + u_{\mathrm{L0},\mathrm{CO}_2} \tag{B.15}$$

where $u_{\mathrm{L},\mathrm{O}_2}(r)$ represents the oxygen liquid recirculation profile calculated with Eqs. (B.8) and (B.14) using just the oxygen flow and $u_{\mathrm{L0},\mathrm{CO}_2}$ denotes the axial liquid velocity for the carbon dioxide flow computed using Eq. (B.14).

B.3.3 Gas hold-up and axial dispersion coefficient prediction

For the average gas holdup estimation, Sotelo et al. (1994) proposed an empirical correlation for air/CO_2 – water systems using micro porous gas diffusers.

$$\bar{\varepsilon}_{\mathrm{G}} = 129 \cdot \left(\frac{U_G \mu_L}{\sigma_{\mathrm{L}}}\right)^{0.99} \left(\frac{\mu_L^4 g}{\rho_L \sigma_L^3}\right)^{-0.123} \left(\frac{\rho_G}{\rho_L}\right)^{0.187} \left(\frac{\mu_G}{\mu_L}\right)^{0.343} \left(\frac{d_o}{D_c}\right)^{-0.089} \tag{B.16}$$

On the other hand, mixing was considered in the model by including an axial dispersion coefficient. The latter was estimated employing the empirical correlation proposed by Kawase and Moo-Young (1986)

$$D_z = 0.343 \cdot D_c^{4/3} \left(g U_{\mathrm{G}}\right)^{1/3} \tag{B.17}$$

B.3.4 Oxygen solubility estimation

Oxygen solubility in water was calculated using Henry's law. The Henry's constant of oxygen in pure water can be estimated using an empirical equation developed in a previous work (Saa et al., 2012),

$$\ln\left(H\right) = -5.9 + \frac{3\cdot 10^3}{T} - \frac{6.9\cdot 10^5}{T^2} \qquad \text{(B.18)}$$

By using Henry's law and the partition constant *m* previously defined, the dissolved oxygen concentration in equilibrium with the bulk gas phase is related by,

$$C_{\mathrm{G}}^{*} = m\cdot C_{\mathrm{L}}^{*} \qquad \text{(B.19)}$$

B.4 Materials and Methods

B.4.1 Experimental set-up

Experiments were carried out in a column 0.3 m in diameter and 1.5 m in height. The bubble column reactor was made of 10 mm thick transparent polymethyl methacrylate, except for the bottom that was made of aluminum. The liquid height was set to H_{L} = 1.2 m and corresponded to tap water. Gas additions were performed using three cylindrical pore diffusers with a pore mean diameter of approximate 20 µm located at the bottom of the reactor in different positions (Fig. B-1). The central diffuser was used to sparge oxygen or nitrogen, while the lateral diffusers were used to inject only carbon dioxide. The gas flow rates sparged in the reactor were measured and controlled using calibrated mass flow controllers FMA-A2407 (Omega Engineering, Inc., Stamford, USA) with flow measurement ranges between 20 to 2000 mL min^{-1}. The equipment used for measuring the

dissolved oxygen concentration was a 3 LCD-trace Fibox v7 machine (PreSens®, Regensburg, Germany), that includes temperature compensation. This optical sensor does not suffer the problems of the Clark's electrode, *e.g.* relatively long response times and oxygen consumption during the measurement (Fernández-Sánchez et al., 2007). In fact, considering that the optical probe response time is at least two orders of magnitude lower than the characteristic time of the process calculated in this work ($k_L a^{-1} > 10^3$ s), the delay of the oxygen probe can be considered small enough to be neglected during the determination of $k_L a$, without affecting the accuracy of the calculations (Gourich et al., 2008; Garcia-Ochoa and Gomez, 2009). The dissolved oxygen kinetics was followed with an optical sensor PSt3 (PreSens®, Regensburg, Germany) with an ideal oxygen measurement range between 0 to 45 mg L^{-1}. The measurements were performed at three different heights: 0.35, 0.77 and 1.15 m from the bottom of the column and at two radial positions: at the center ($r = 0$) and at the wall ($r = R$). For the measurements at the wall, mini planar sensors (spots) were glued to the column wall and then employed to measure the oxygen concentration inside the reactor by using an external fiber optic probe. In the case of the center measurements, a stainless steel tubing (1 cm diameter and 1.2 m long) was introduced into the column, allowing guiding and safely placing in a fix location the oxygen dipping probe. The measurements at the six locations were carried out in triplicate and conducted at room temperature (20°C) and atmospheric pressure.

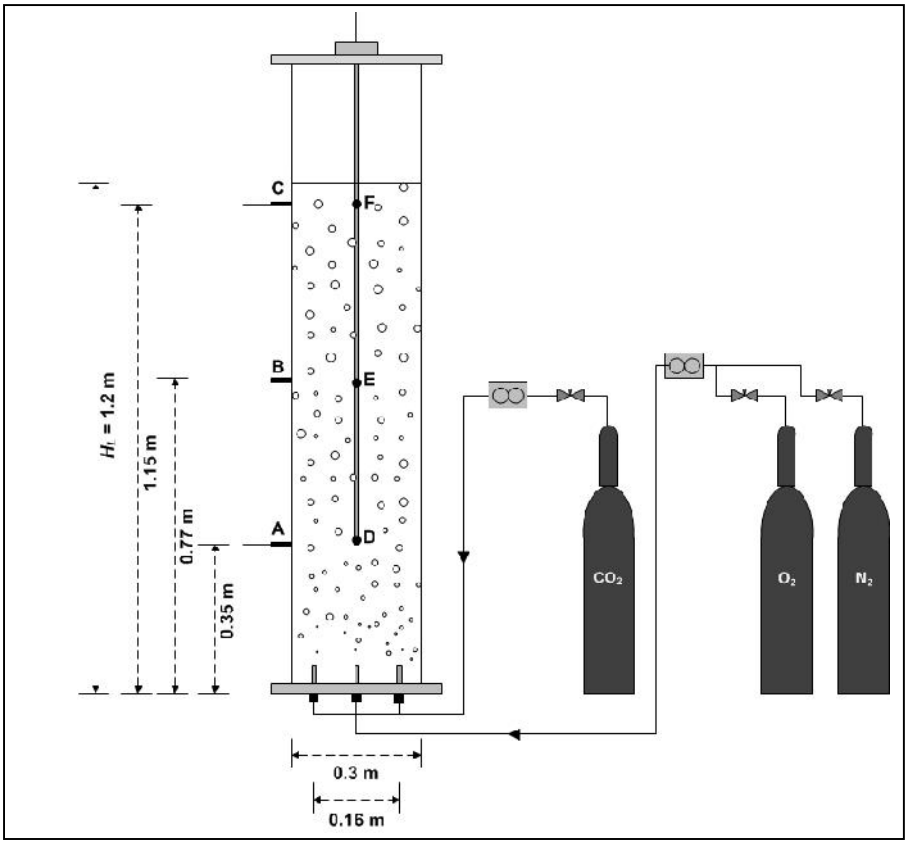

Figure B-1: Details of the experimental set-up. Letters **A**, **B**, **C**, **D**, **E**, and **F** denote different probe locations for the dissolved oxygen measurements

B.4.2 Oxygen pulse additions and $k_L a$ determination

Oxygen pulse additions were carried out without, *i.e.* control case, and with carbon dioxide injection. In the control case, all dissolved gases were desorbed by a nitrogen injection of 700 mL min^{-1} until oxygen concentrations lower than 0.5 mg L^{-1} were reached in the column. Then, the nitrogen flow was stopped and a flow of 250 mL min^{-1} pure oxygen was injected during 5 min. The choice of the oxygen flow was estimated in order to yield an oxygen transfer rate of 1 mg O_2 L^{-1} min^{-1}, which corresponds to a commonly employed specific rate during wine fermentations (Sablayrolles et al., 1996).The influence

of the simultaneous dissolved carbon dioxide on the volumetric mass transfer coefficient was then, also assessed using this method. Instead of desorption with nitrogen, two different carbon dioxide flow rates of 350 mL min^{-1} and 700 mL min^{-1} were used, emulating carbon production rates of 0.46 and 0.91 g L^{-1} h^{-1}, respectively. Oxygen desorption with carbon dioxide in the column takes longer than with nitrogen (approx. 2 hours), which allowed reaching carbon dioxide saturation concentrations up to 1.7 g L^{-1} at 20°C in the liquid phase (Perry and Green, 1997). When the oxygen concentration level reached 0.5 mg L^{-1}, pure oxygen flow of 250 mL min^{-1} was injected simultaneously during 5 min, without stopping the carbon dioxide flow. In each case, $k_L a$ were determined by fitting the experimental dissolved oxygen data to the proposed model at the six locations indicated in Figure B-1.

B.4.3 Oxygen solubility

Solubility experiments were performed following the methodology employed for determining the $k_L a$ values, except that in this case, oxygen additions were carried until oxygen saturation was achieved. The oxygen flow - as well as the carbon dioxide flows - used in this case were the same as those previously mentioned. Dissolved oxygen concentration in the liquid phase was measured using only the oxygen probe located in position F (Fig. B-1). Equilibrium concentrations were recorded when dissolved oxygen concentration variations were less than ±1%. These values were then employed to estimate the oxygen concentrations in the gas phase at the inlet (Eq. B.7) by using Eq. (B.19) for each addition.

B.4.4 Numerical resolution

The partial differential equations were solved employing the Method of Lines (MOL) (Schiesser, 1991). The spatial derivatives of the model were computed using second-order central finite differences. We divided both the liquid phase and the gas phase in 121 nodes, resulting in a system of 242 ordinary differential equations. This discretization scheme was used to solve the dissolved oxygen profile as a function of the height for different radial positions. We solved the resulting time-dependent equations using the *ode15s* solver of MATLAB® in a personal computer with an Intel Core i5 @ 2.26 GHz processor and 3 GB of RAM.

B.4.5 Parameter fitting

The volumetric oxygen mass transfer coefficient was estimated by minimizing the sum of squared residual errors between predicted and experimental data weighted by the standard deviation of the measurements,

$$\underset{k_L a}{\text{Min}} \sum_{k}^{N} \left(\frac{C_L^{\text{model}} - C_L^{\text{meas}}}{\pm_k} \right)^2 \tag{B.21}$$

where C_L^{model} is the dissolved oxygen concentration predicted, C_L^{meas} is the dissolved oxygen concentration measured, $\pm_k$ denotes the standard deviation of the measurement k and N represents the number of measurements. Dynamic optimization of the estimated $k_L a$ values was carried out using *fminsearch* MATLAB® function that is a robust derivative-free method for unconstrained multivariable optimization.

B.4.5 Statistics

To calculate the 95% confidence intervals for the estimated parameters, the MATLAB® function *nlparci* was employed as described by Saa et al. (2012).

B.5 Results and discussion

B.5.1 Oxygen saturation concentration with simultaneous carbon dioxide injection

$k_L a$ estimation during oxygen pulse additions under a given operational condition requires the oxygen saturation concentration C_L^*, as it is necessary to estimate the oxygen concentrations in the gas phase at the inlet which can be computed by $C_{G,0} = m \cdot C_L^*$. Table B-1 shows the experimental oxygen saturation values obtained under the conditions studied.

Table B-1: Oxygen solubility using different carbon dioxide flows at 20°C

Experiment	Injected gas flow	C_L^* [mg O_2 L^{-1}]	$C_{G,0}$ [mg O_2 L^{-1}]
Control case	250 mL min^{-1} O_2	33.1	979.4
CO_2 addition 1	250 mL min^{-1} O_2 + 350 mL min^{-1} CO_2	10.3	303.3
CO_2 addition 2	250 mL min^{-1} O_2 + 700 mL min^{-1} CO_2	6.8	201.3

The saturation value obtained for the control case is lower than values reported for saturation experiments with pure water (Devatine et al., 2007), although it agrees well with saturation values of around 32 mg L^{-1} employed using tap water under similar conditions (Gourich et al., 2006, 2008). As expected, increasing the carbon dioxide flow decreases the oxygen saturation concentration as it dilutes the oxygen in the gas phase. Experimental

data show a decrease on the oxygen concentration in the gas phase of around 80% for maximum CO_2 flow. Similar observations were reported recently (Devatine et al., 2007; Devatine and Mietton-Peuchot, 2009; Chiciuc et al., 2010), although these works studied only the effect of dissolved carbon dioxide presence on the oxygen mass transfer. These results highlight the importance of continuous carbon dioxide flow upon oxygen saturation concentration as it affects significantly the oxygen equilibrium and the model boundary condition (B.7).

B.5.2 Oxygen dissolution during oxygen additions without carbon dioxide injection

Before estimating the $k_L a$ value, it is necessary to determine first the time lag between the change in the gas composition and the effective measurement at the probe location, as it affects the $k_L a$ determination. As pointed by Gourich et al. (2008), this time is composed by the combined effect of several characteristic times related mainly to the probe dynamics and the reestablishment of the hydrodynamic steady state condition. In our case, the probe dynamics does not play a significant role as it is much faster than the process dynamics; hence, the observed time lag is probably associated only with the establishment of the steady state condition. The observed time lag in this condition was around 50 s for the center and the border of the column, which agrees with experimentally determined mixing times ranging between 10 – 100 s in bubble column reactors (Choi et al., 1996).

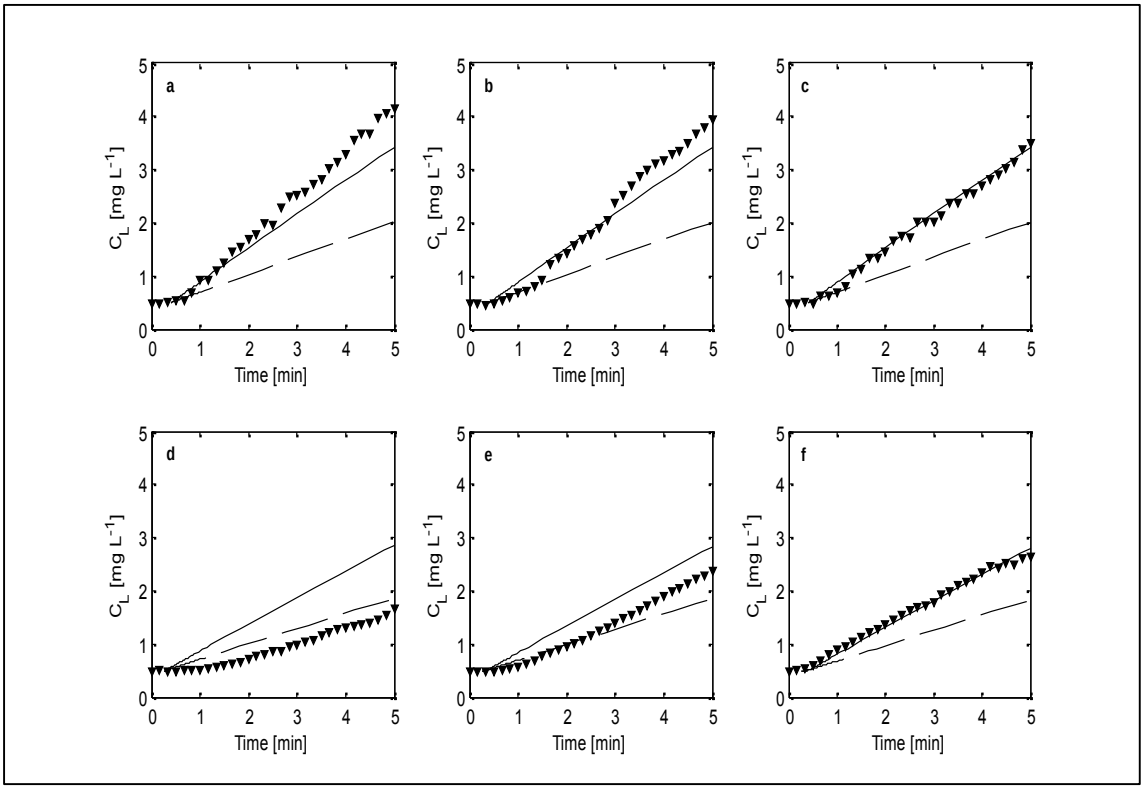

Figure B-2: Kinetics of oxygen dissolution without carbon dioxide injection at different positions throughout the column. Figures **a**, **b** and **c** show measurements (black triangles) at different heights at the center (**a**. z = 0.35 m, **b**. z = 0.77 m and **c**. z = 1.15 m) and at the wall (**d**. z = 0.35 m, **e**. z = 0.77 m and **f**. z = 1.15 m) of the column. The solid line represents model predictions with the fitted $k_L a$ value, while the dashed line illustrates the model predictions with the $k_L a$ value predicted by Eq. (B.22).

Once the time lag was determined, $k_L a$ estimation was carried out. The fitted $k_L a$ value was $3.5 \cdot 10^{-4} \pm 0.5 \cdot 10^{-4}$ s^{-1}. Model fittings at different heights and radii are illustrated

in Figure B-2. The mean relative error of the model was 16.9% compared to experimental data. To compare the quality of the estimated $k_L a$ value, a commonly employed correlation for $k_L a$ prediction was used (Akita and Yoshida, 1973).

$$k_L a = \left(\frac{0.6 D_L}{D_c^2} \right) \left(\frac{\neg_L}{D_L} \right)^{0.5} \left(\frac{g D_c^{2} \circ_L}{¥_L} \right)^{0.62} \left(\frac{g D_c^3}{\neg_L^2} \right)^{0.31} £_G^{1.1} \qquad \text{(B.22)}$$

Prediction of the $k_L a$ value with Eq. (B.22) yields $1.8 \cdot 10^{-4}$ s^{-1}, which is a poor prediction for the estimated $k_L a$ value (48.6% relative error). This result can be explained because of the range of applicability of the employed correlation, which is far below the studied case. This correlation was developed for predicting $k_L a$ values using gas superficial velocities from $4 \cdot 10^{-3}$ m s^{-1}, while in this case oxygen gas velocity value is around $6 \cdot 10^{-5}$ m s^{-1}. Nevertheless, the correlation performance is expected to improve when the carbon dioxide injection is carried out, as the superficial gas superficial velocity is increased.

Satisfactory fittings were obtained using the fitted $k_L a$ in the top and center of the column, unlike the case when the predicted value was used (Fig. B-2a, B-2b and B-2c). Mean relative differences with experimental data were less than 11% in the center of the column using the fitted value. It is also worth noting, that the dissolved oxygen values reached in the center of the column are significantly higher than the values observed in the border. The latter clearly shows the prevalence of dissolved oxygen radial gradients over axial gradients during the addition, which has been already reported by Adoua et al. (2010) during micro-oxygenation simulations under similar conditions.

On the contrary, model fittings obtained in the border of the column were not as satisfactory as in the center (Fig. B-2d, B-2e and B-2f). Higher discrepancies between the model and experimental data are observed in the top of the column, where the model significantly overestimates the dissolved oxygen concentration (Fig. B-2d). This difference can be explained by inaccuracies in predicting the hydrodynamics of the column, as the employed correlations assume a flat developed velocity profile that depends only on the radial position and not on the axial position (Wu and Al-Dahhan, 2001). Results reported by Reese and Fan (1994) show that entrance effects are significant in the dispersed bubble regime but diminish with increasing velocity, especially in the coalesced bubble regime. Thus, at low superficial gas velocities the hydrodynamics is not well predicted, particularly in the borders where the liquid velocity is minimum (Adoua et al., 2010), because of the relative higher entrance-length required for the flow development. Nevertheless, model predictions are still acceptable as they satisfactorily reproduce the evolution of dissolved oxygen in the center of the column.

B.5.3 Oxygen dissolution during oxygen additions with carbon dioxide injection

Figure B-3 and B-4 show the different model fittings obtained during oxygen pulse additions with simultaneous carbon dioxide injections of 350 and 700 mL min^{-1}, respectively. In these cases, the time lag was shorter than the previous case and different for each radial position. In the center of the column, time lags of 10 to 15 s were observed; while in the border of the column, they were around 40 s. The difference with the control case can be explained by the fact that the oxygen pulses were performed simultaneously

with the carbon dioxide injection, unlike the previous case where the nitrogen injection was stopped before the oxygen addition. The latter could shorten the time lag as the establishment of the hydrodynamic condition was not so pronounced.

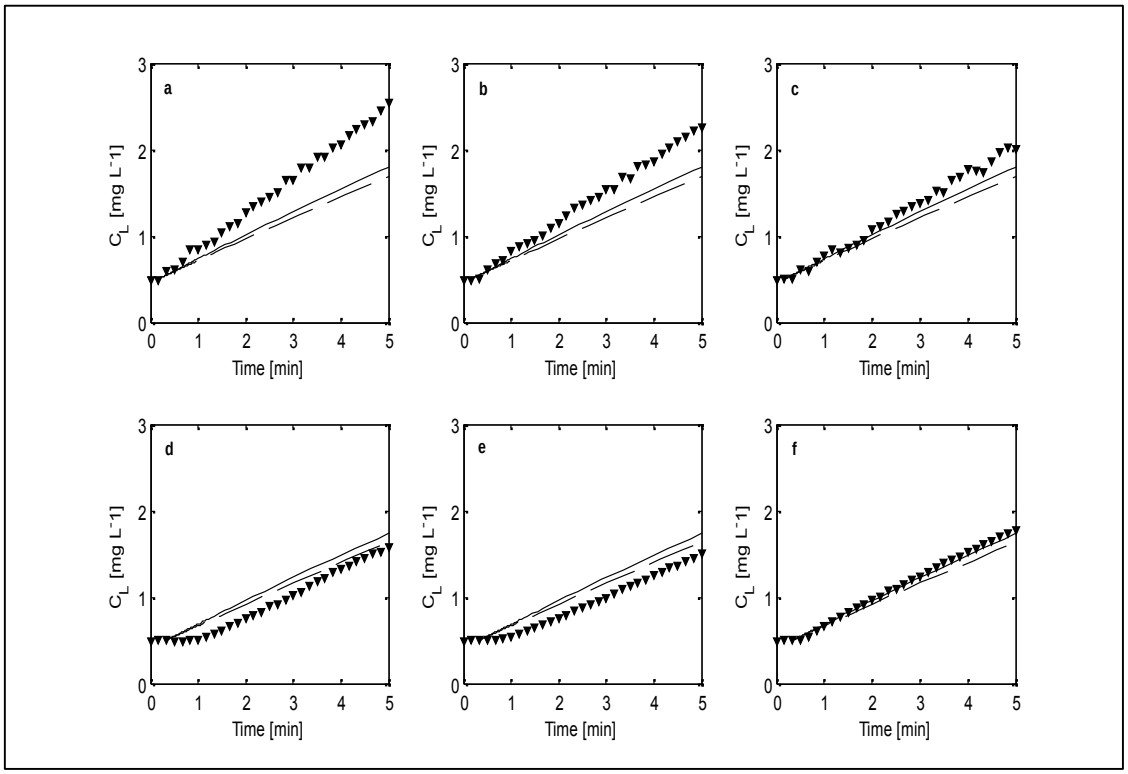

Figure B-3: Kinetics of oxygen dissolution with 350 mL min^{-1} carbon dioxide injection at different positions throughout the column. Figures **a**, **b** and **c** show measurements (black triangles) at different heights at the center (**a**. z = 0.35 m, **b**. z = 0.77 m and **c**. z = 1.15 m) and at the wall (**d**. z = 0.35 m, **e**. z = 0.77 m and **f**. z = 1.15 m) of the column. The solid line represents model predictions with the fitted $k_L a$ value, while the dashed line illustrates the model predictions with the $k_L a$ value predicted by Eq. (B.22)

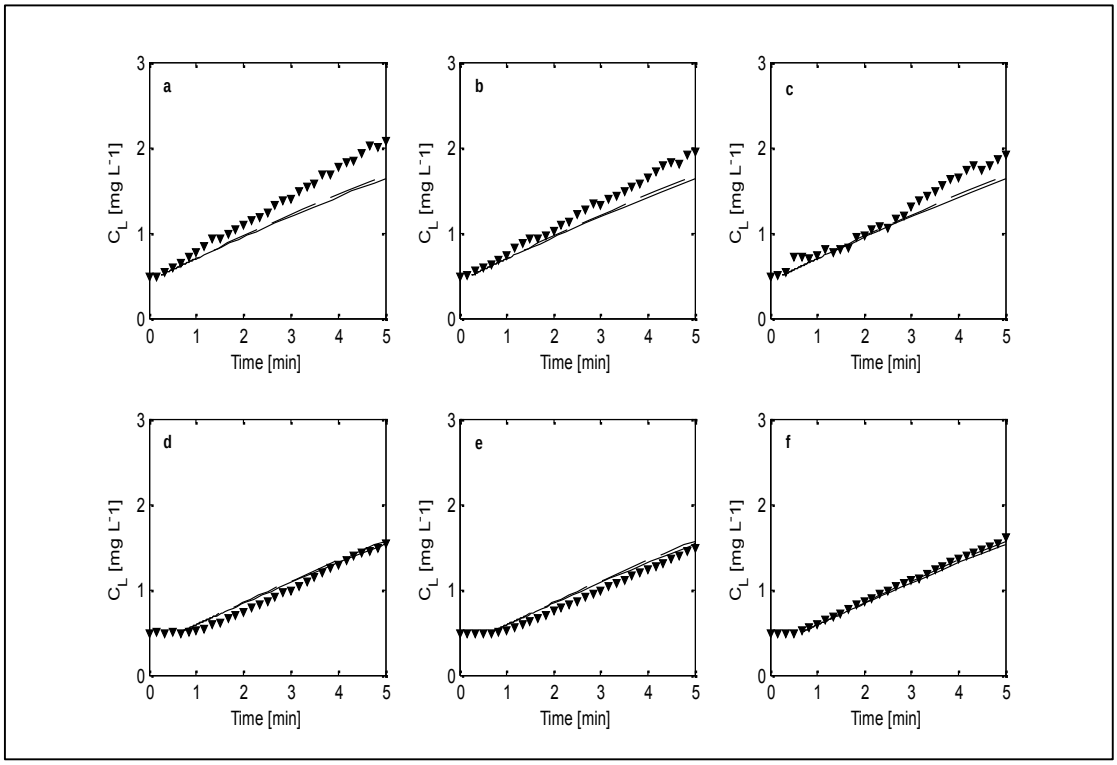

Figure B-4: Kinetics of oxygen dissolution with 700 mL min^{-1} carbon dioxide injection at different positions throughout the column. Figures **a**, **b** and **c** show measurements (black triangles) at different heights at the center (**a**. z = 0.35 m, **b**. z = 0.77 m and **c**. z = 1.15 m) and at the wall (**d**. z = 0.35 m, **e**. z = 0.77 m and **f**. z = 1.15 m) of the column. The solid line represents model predictions with the fitted k_La value, while the dashed line illustrates the model predictions with the k_La value predicted by Eq. (B.22)

Model fittings with CO_2 injections using the fitted and predicted k_La agree fairly well with experimental data. Fitted and predicted k_La values show good agreement, contrary to the previous case (Table B-2). Better predictions in these two cases could be

explained because gas superficial velocities employed are closer to the range of applicability of Eq. (B.22). Results show that the increase on the gas injection increases the estimated $k_L a$ values, which is consistent with a previous report on the positive effect of increasing the gas superficial velocity on the volumetric mass transfer coefficient and the gas holdup under homogeneous bubbly regime (Kantarci et al., 2005). The increased superficial gas velocity due to CO_2 injection increases the turbulence intensity, enhancing the mass transfer coefficient k_L as well as the number of bubbles as more gas is being injected; as a result, the gas holdup, and therefore the specific interfacial area a, increases (Garcia-Ochoa and Gomez, 2009). When combining both effects, the net result yields an increase in the $k_L a$, as observed experimentally.

Table B-2: Fitted and predicted $k_L a$ under the studied conditions

Experiment	Fitted volumetric mass transfer coefficient, $k_L a \cdot 10^{-4}$ [s^{-1}]	Predicted volumetric mass transfer coefficient, $k_L a \cdot 10^{-4}$ [s^{-1}]	Relative error (%)
Control case	3.5 ± 0.5	1.8	48.6
CO_2 addition 1	5.0 ± 0.6	4.5	11.1
CO_2 addition 2	7.2 ± 0.8	7.5	4.2

Furthermore, satisfactory fittings were obtained in both, the center and the border of the column (Fig. B-3 and B-4). Mean relative differences with the dissolved oxygen evolution data were less than 10.2% for the case with carbon dioxide injection of 350 mL min^{-1}, and even lower for the case of 700 mL min^{-1} injection (approx. 8.2%). These results show the suitability of the model for estimating the dissolved oxygen evolution with carbon dioxide injection. The improvement of the model performance is probably due to

the decrease on the entrance effects as the increased gas injections generates greater liquid velocities (Reese and Fan, 1994), and the estimation of the liquid velocity profile. Indeed, dissolved oxygen values reached in the center of the column are a bit higher than the values observed at the wall for all heights; however the difference is not as notorious as the case without carbon dioxide injection. Thus, dissolved oxygen radial profiles are more homogenous throughout the column, which is a result of a more uniform flow due to the distributed injection (Mudde et al., 2009). The latter effect can be described using Eq. (B.15), which explains the satisfactory results.

Finally, it is noteworthy that experimental dissolved oxygen evolution profiles show a decrease of the oxygen concentration values reached after the oxygen pulse, compared to the control case (Fig. B-2, B-3 and B-4). Dissolved oxygen levels achieved when carbon dioxide injections of 350 and 700 mL min^{-1} were performed were similar, reaching around 38% and 25% lower dissolved oxygen values for central and lateral positions, respectively. Hence, although carbon dioxide injections enhance the volumetric mass transfer coefficient, its negative effect on the oxygen solubility prevails as the oxygen levels reached are lower.

B.5.4 Influence of simultaneous carbon dioxide injection on the oxygen dissolution rate

The effect of the carbon dioxide injection upon the oxygen dissolution rate has several effects; on one hand, the carbon dioxide injection decreases the oxygen solubility as it dilutes the oxygen in the gas phase, and, on the other hand, it increases the gas superficial velocity which increases the $k_L a$, the liquid velocity and the axial dispersion

coefficient. In order to analyze these effects, Table B-3 compares different oxygen dissolution terms considered in the modeling.

Table B-3: Comparison of different oxygen dissolution terms

Experiment	Mean liquid velocity (advection), $\bar{u}_L$ [m s^{-1}]	Axial dispersion coefficient (dispersion), D_z [m^2 s^{-1}]	Maximum O_2 transferable flux (convection), $k_L a \cdot C_{G,0}/m$
Control case	0.2	$1.8 \cdot 10^{-7}$	$10.1 \cdot 10^{-3}$
CO_2 addition 1	1.4	$4.3 \cdot 10^{-7}$	$4.9 \cdot 10^{-3}$
CO_2 addition 2	1.9	$6.8 \cdot 10^{-7}$	$4.5 \cdot 10^{-3}$

As indicated in Table B-3, the most important variables involved in oxygen dissolution are convective and advective transport, which are several orders of magnitude higher than the dispersive term. Indeed, reported data indicates a minor role of the dispersion coefficient on the volumetric mass transfer coefficient determination under similar conditions (Gourich et al., 2006, 2008).

Experimental results revealed that the negative effect of CO_2 injections is predominant on the oxygen dissolution rate, which indicates that the convective term is the most important. The latter considers two aspects: oxygen equilibrium and oxygen transfer rate. Observed data shows that the negative effect of CO_2 on the oxygen solubility is more important. Indeed, CO_2 presence dramatically decreases the oxygen dissolution rate by at least 50% for the conditions studied, reaching a 56% decrease for the maximum CO_2 injection. Similar results have been reported for oxygen additions with dissolved carbon dioxide simulating micro-oxygenation conditions (Devatine et al., 2007; Devatine and Mietton-Peuchot, 2009; Chiciuc et al., 2010). Results also show that, regardless of the

carbon dioxide flow employed, the decrease of the oxygen dissolution rate is similar. Thus, the dissolved carbon dioxide presence is by far the most important aspect that should be taken into account during oxygen additions under emulated oenological conditions.

B.6 Conclusions

In this work, an oxygen mass balance model including liquid recirculation and mixing has been developed for modeling the dissolved oxygen evolution during pulse additions with simultaneous CO_2 continuous injection in a bubble column. The proposed model reproduced accurately the dissolved oxygen profiles observed during the oxygen additions. Experimental and model results showed that CO_2 injection increases the $k_L a$ value from $3.5 \cdot 10^{-4}$ to $7.2 \cdot 10^{-4}$ s^{-1} for maximum CO_2 injection rate, but simultaneously reduces the oxygen solubility in the liquid phase by 80%, as it dilutes the oxygen fraction in the gas phase. The latter effect has shown to be more important, which explains the decrease of almost 60% on the oxygen dissolution rate when simulating a CO_2 production rate of 0.9 g L^{-1} h^{-1}. The proposed model will help designing better oxygen addition systems for industrial wine fermentations.

REFERENCES

Adoua, R., Mietton-Peuchot, M., Milisic, V., 2010. Modeling of oxygen transfer in wines. Chemical Engineering Science 65, 5455–5463.

Akita, K., Yoshida, F., 1973. Gas Holdup and Volumetric Mass Transfer Coefficient in Bubble Columns. Effects of Liquid Properties. Industrial & Engineering Chemistry Process Design and Development 12, 76–80.

Atanasova, V., Fulcrand, H., Cheynier, V., Moutounet, M., 2002. Effect of oxygenation on polyphenol changes occurring in the course of wine-making. Analytica Chimica Acta 458, 15–27.

Blateyron, L., Aguera, E., Dubois, C., Gerland, C., Sablayrolles, J.M., 1998. Control of oxygen additions during alcoholic fermentations. Wein-Wissenschaft 53, 131–135.

Blayteron, L. and Sablayrolles, J., 2001. Stuck and slow fermentations in enology: statistical study of causes and effectiveness of combined additions of oxygen and diammonium phosphate. Journal of Bioscience and Bioengineering 91, 184–189.

Bonate, P.L., 2011. Pharmacokinetic-Pharmacodynamic Modeling and Simulation, Health (San Francisco). Springer US, Boston, MA.

Boulton, R., Singleton, V., Bisson, L., Kunkee, R., 1996. Principles and Practices of Winemaking. Chapman Hall, New York.

Burke, P.V., Kwast, K.E., Everts, F., Poyton, R.O., 1998. A fermentor system for regulating oxygen at low concentrations in cultures of Saccharomyces cerevisiae. Applied and environmental microbiology 64, 1040–4.

Cachaza, E.M., Díaz, M.E., Montes, F.J., Gala, M.A., 2008. Analytical Solution of the Mass Conservation Equations in Gas-Liquid Systems : Applicability to the Evaluation of the Volumetric Mass Transfer Coefficient (kLa). Ind. Eng. Chem. Res. 47, 4510–4522.

Calik, G., Vural, H., Ozdamar, T., 1997. Bioprocess parameters and oxygen transfer effects in the growth of Pseudomonas dacunhae for L-alanine production. Biotechnology and Bioengineering 65, 109–116.

Cargill R.W., 1993. The Solubility of Gases in Water-Alcohol Mixtures. Chemical Society Reviews 135–141.

Casalta, E., Aguera, E., Picou, C., Rodriguez-Bencomo, J.-J., Salmon, J.-M., Sablayrolles, J.-M., 2010. A comparison of laboratory and pilot-scale fermentations in winemaking conditions. Applied microbiology and biotechnology 87, 1665–1673.

Casas López, J.L., Rodríguez Porcel, E.M., Oller Alberola, I., Ballesteros Martin, M.M., Sánchez Pérez, J. a., Fernández Sevilla, J.M., Chisti, Y., Lo, J.L.C., Alberola, I.O., Martin, M.M.B., Sa, J.A., Ferna, J.M., North, P., Zealand, N., 2006. Simultaneous Determination of Oxygen Consumption Rate and Volumetric Oxygen Transfer Coefficient in Pneumatically Agitated Bioreactors. Industrial & Engineering Chemistry Research 45, 1167–1171.

Castellari, M., Simonato, B., Tornielli, G.B., Spinelli, P., Ferrarini, R., 2004. Effects of different enological treatments on dissolved oxygen in wines. Italian journal of food science 16, 387–396.

Castiñeira, a., Peña, R.M., Herrero, C., García-Martín, S., 2002. Analysis of Organic Acids in Wine by Capillary Electrophoresis with Direct UV Detection. Journal of Food Composition and Analysis 15, 319–331.

Caşcaval, D., Galaction, A.-I., Turnea, M., 2011. Comparative analysis of oxygen transfer rate distribution in stirred bioreactor for simulated and real fermentation broths. Journal of industrial microbiology & biotechnology 38, 1449–1466.

Chiciuc, I., Farines, V., Mietton-Peuchot, M., Devatine, A., 2010. Effect of wine properties and operating mode upon mass transfer in micro-oxygenation. International Journal of Food Engineering 6.

Choi, K., Chisti, Y., Moo-Young, M., 1996. Comparative evaluation of hydrodynamic and gas-liquid mass transfer characteristics in bubble column and airlift slurry reactors. The Chemical Engineering Journal and the Biochemical Engineering Journal 62, 223–229.

Degenring, D., 2004. Sensitivity analysis for the reduction of complex metabolism models. Journal of Process Control 14, 729–745.

Devatine, A., Chiciuc, I., Poupot, C., Mietton-Peuchot, M., 2007. Micro-oxygenation of wine in presence of dissolved carbon dioxide. Chemical Engineering Science 62, 4579–4588.

Devatine, A., Mietton-Peuchot, M., 2009. A mathematical approach for oxygenation using micro bubbles Application to the micro-oxygenation of wine. Chemical Engineering Science 64, 1909–1917.

Dhaouadi, H., Poncin, S., Hornut, J.M., Midoux, N., 2008. Gas–liquid mass transfer in bubble column reactor: Analytical solution and experimental confirmation. Chemical Engineering and Processing: Process Intensification 47, 548–556.

Djelal, H., Larher, F., Martin, G., Amrane, A., 2006. Effect of the dissolved oxygen on the bioproduction of glycerol and ethanol by Hansenula anomala growing under salt stress conditions. Journal of biotechnology 125, 95–103.

Doran, P., 1995. Bioprocess Engineering Principles. Academic Press, London.

Eya, H., Mishima, K., Nagatani, M., Iwai, Y., Arai, Y., 1994. Measurement and correlation of solubilities of oxygen in aqueous solutions containing glucose, sucrose and maltose. Fluid Phase Equilibria 97, 201–209.

Fernández-Sánchez, J.F., Roth, T., Cannas, R., Nazeeruddin, M.K., Spichiger, S., Graetzel, M., Spichiger-Keller, U.E., 2007. Novel oxygen sensitive complexes for optical oxygen sensing. Talanta 71, 242–250.

Fornairon-Bonnefond, C., Demaretz, V., Rosenfeld, E., Salmon, J., 2002. Oxygen addition and sterol synthesis in Saccharomyces cerevisiae during enological fermentation. Journal of Bioscience and Bioengineering 93, 176–182.

Gagnon, H., Lounes, M., Thibault, J., 1998. Power Consumption and Mass Transfer in Agitated Gas-Liquid columns: A Comparative Study. The Canadian Journal of Chemical Engineering 76, 379–389.

Garcia-Calvo, E., Letón, P., 1994. Prediction of fluid dynamics and liquid mixing in bubble columns. Chemical Engineering Science 49, 3643–3649.

Garcia-Ochoa, F., Castro, E., Santos, V., 2000. Oxygen transfer and uptake rates during xanthan gum production. Enzyme and microbial technology 27, 680–690.

Garcia-Ochoa, F., Gomez, E., 2009. Bioreactor scale-up and oxygen transfer rate in microbial processes: an overview. Biotechnology advances 27, 153–76.

Garcia-Ochoa, F., Gomez, E., Santos, V.E., Merchuk, J.C., 2010. Oxygen uptake rate in microbial processes: An overview. Biochemical Engineering Journal 49, 289–307.

Gourich, B., Vial, C., El Azher, N., Belhaj Soulami, M., Ziyad, M., 2006. Improvement of oxygen mass transfer estimation from oxygen concentration measurements in bubble column reactors. Chemical Engineering Science 61, 6218–6222.

Gourich, B., Vial, C., El Azher, N., Belhaj Soulami, M., Ziyad, M., 2008. Influence of hydrodynamics and probe response on oxygen mass transfer measurements in a high aspect ratio bubble column reactor: Effect of the coalescence behaviour of the liquid phase. Biochemical Engineering Journal 39, 1–14.

Gros, J., Dussap, C., Catté, M., 1999. Estimation of O(2) and CO(2) Solubility in Microbial Culture Media. Biotechnology progress 15, 923–927.

Gupta, P., Ong, B., Al-dahhan, M.H., Dudukovic, M.P., Toseland, B.A., 2001. Hydrodynamics of churn turbulent bubble columns : gas – liquid recirculation and mechanistic modeling. Catalysis Today 64, 253–269.

Ingalls, B., 2003. Sensitivity analysis of stoichiometric networks: an extension of metabolic control analysis to non-steady state trajectories. Journal of Theoretical Biology 222, 23–36.

Jamnongwong, M., Loubiere, K., Dietrich, N., Hébrard, G., 2010. Experimental study of oxygen diffusion coefficients in clean water containing salt, glucose or surfactant: Consequences on the liquid-side mass transfer coefficients. Chemical Engineering Journal 165, 758–768.

Kantarci, N., Borak, F., Ulgen, K.O., 2005. Bubble column reactors. Process Biochemistry 40, 2263–2283.

Kawase, Y., Moo-Young, M., 1986. Liquid phase mixing in bubble columns with Newtonian and non-Newtonian fluids. Chemical Engineering Science 41, 1969–1977.

Kutsche, I., Gildehaus, G., Schuler, D., Schumpe, A., 1984. Oxygen solubilities in aqueous alcohol solutions. Society 29, 286–287.

Lemoine, R., Behkish, A., Sehabiague, L., Heintz, Y.J., Oukaci, R., Morsi, B.I., 2008. An algorithm for predicting the hydrodynamic and mass transfer parameters in bubble column and slurry bubble column reactors. Fuel Processing Technology 89, 322–343.

Linek, V., Kordač, M., Moucha, T., 2005. Mechanism of mass transfer from bubbles in dispersions. Chemical Engineering and Processing: Process Intensification 44, 121–130.

Luhring, P., Schumpe, A., 1989. Gas solubilities (H2, He , N2, CO, O2, Ar, CO2) in organic liquids at 293.2 K. J. Chem. Eng. Data 34, 250–252.

Merchuk, J., 1977. Further considerations on the enhancement of oxygen transfer in fermentation broths. Biotechnology and Bioengineering 19, 1885–1889.

Mishima, K., Matsuo, N., Kawakami, A., Komorita, N., Nagatani, M., Ouchi, M., 1996. Measurement and correlation of solubilities of oxygen in aqueous solutions containing galactose and fructose. Fluid Phase Equilibria 118, 221–226.

Moo-Young, M., Blanch, H., 1981. Design of Biochemical Reactors Mass Transfer Criteria for Simple and Complex Systems. Advances in Biochemical EngineeringBiotechnology 19, 1–69.

Morakul, S., Mouret, J.-R., Nicolle, P., Trelea, I.C., Sablayrolles, J.-M., Athes, V., 2011. Modeling of the gas–liquid partitioning of aroma compounds during wine alcoholic fermentation and prediction of aroma losses. Process Biochemistry 46, 1125–1131.

Mudde, R.F., Harteveld, W.K., Van den Akker, H.E.A., 2009. Uniform flow in bubble columns. Ind. Eng. Chem. Res. 48, 148–158.

Oszmianski, J., Moutounet, M., Polyme, L., 1996. Iron-Catalyzed Oxidation of (+) -Catechin in Model Systems 1712–1715.

Perry, R.., Green, D.W., 1997. Perry's Chemical Engineers' Handbook., 7th ed. McGraw-Hill, New York.

Pyrzyńska, K., 2004. Analytical Methods for the Determination of Trace Metals in Wine. Critical Reviews in Analytical Chemistry 34, 69–83.

Pérez-Magariño, S., Sánchez-Iglesias, M., Ortega-Heras, M., González-Huerta, C., González-Sanjosé, M.L., 2007. Colour stabilization of red wines by microoxygenation treatment before malolactic fermentation. Food Chemistry 101, 881–893.

Rasmussen, H., 2003. Oxygen solubilities of media used in electrochemical respiration measurements. Analytical Biochemistry 319, 105–113.

Reese, J., Fan, L., 1994. Transient flow structure in the entrance region of a bubble column using particle image velocimetry. Chemical Engineering Science 49, 5623–5636.

Rettich, T., 2000. Solubility of gases in liquids. 22. High-precision determination of Henry's law constants of oxygen in liquid water fromT = 274 K to T = 328 K. The Journal of Chemical Thermodynamics 32, 1145–1156.

Ribéreau-Gayon, P., Dubourdieu, D., Donèche, B., Lonvaud, A., 2006. Handbook of enology volume 1 The microbiology of wine and vinifications, 2nd ed. Wiley, Hoboken.

Rischbieter, E., Schumpe, A., Wunder, V., 1996. Gas Solubilities in Aqueous Solutions of Organic Substances. Journal of Chemical & Engineering Data 41, 809–812.

Rosenfeld, E., Beauvoit, B., Blondin, B., Salmon, J., 2003. Oxygen Consumption by Anaerobic Saccharomyces cerevisiae under Enological Conditions : Effect on Fermentation Kinetics Oxygen Consumption by Anaerobic Saccharomyces cerevisiae under Enological Conditions : Effect on Fermentation Kinetics.

Rosenfeld, E., Beauvoit, B., Rigoulet, M., Salmon, J.-M., 2002. Non-respiratory oxygen consumption pathways in anaerobically-grown Saccharomyces cerevisiae: evidence and partial characterization. Yeast (Chichester, England) 19, 1299–321.

Rosenfeld, E., Schaeffer, J., Beauvoit, B., Salmon, J.-M., 2004. Isolation and properties of promitochondria from anaerobic stationary-phase yeast cells. Antonie van Leeuwenhoek 85, 9–21.

Rubio, F.C., Garcia, J.L., Molina, E., Chisti, Y., 1999. Steady-state axial profiles of dissolved oxygen in tall bubble column bioreactors. Chemical Engineering Science 54, 1711–1723.

Rubio, F.C., Mirón, A.S., García, M.C.C., Camacho, F.G., Grima, E.M., Chisti, Y., 2004. Mixing in bubble columns: a new approach for characterizing dispersion coefficients. Chemical Engineering Science 59, 4369–4376.

Ruthiya, K.., van der Schaaf, J., Kuster, B.F.., Schouten, J.., 2003. Mechanisms of physical and reaction enhancement of mass transfer in a gas inducing stirred slurry reactor. Chemical Engineering Journal 96, 55–69.

Saa, P.A., Moenne, M.I., Pérez-Correa, J.R., Agosin, E., Moenne, I., Pérez-Correa, R., 2012. Modeling oxygen dissolution and biological uptake during pulse oxygen additions in oenological fermentations. Bioprocess and biosystems engineering 35, 1167–1178.

Sablayrolles, J., Barre, P., 1986. Evaluation des besoins en oxygene de fermentations alcooliques en conditions oenologiques simulees. Sci. Alim. 6, 373–383.

Sablayrolles, J.-M., Dubois, C., Manginot, C., Roustan, J.-L., Barre, P., 1996. Effectiveness of combined ammoniacal nitrogen and oxygen additions for completion of sluggish and stuck wine fermentations. Journal of Fermentation and Bioengineering 82, 377–381.

Sacher, J., Saa, P., Cárcamo, M., López, J., Gelmi, C., Pérez-Correa, R., 2011. Improved calibration of a solid substrate model. Electronic Journal of Biotechnology 14.

Salmon, J., 2006. Interactions between yeast, oxygen and polyphenols during alcoholic fermentations: Practical implications. LWT - Food Science and Technology 39, 959–965.

Salmon, J.M., Barre, P., 1998. Improvement of nitrogen assimilation and fermentation kinetics under enological conditions by derepression of alternative nitrogen-assimilatory pathways in an industrial Saccharomyces cerevisiae strain. Applied and environmental microbiology 64, 3831–7.

Schiesser, W.E., 1991. The numerical method of lines: integration of partial differential equations. Academic Press, Inc., San Diego.

Schumpe, A., Quicker, G., Deckwer, W.D., 1982. Gas solubilities in microbial culture media. Advances in Biochemical Engineering/Biotechnology 24, 1–38.

Schwacke, J., Voit, E., 2005. Computation and analysis of time-dependent sensitivities in Generalized Mass Action systems. Journal of Theoretical Biology 236, 21–38.

Silva, A., Lambri, M., 2006. Oxygen measures and consumption in must and wine. Analytica Chimica Acta 563, 391–395.

Singleton, V.L., 1987. Oxygen with phenols and related reactions in musts, wines and model systems: observations and practical implications. American Journal of Enology and Viticulture 38, 69–77.

Singleton, V.L., 2000. A survey of wine aging reactions, especially with oxygen, in: Proceedings of the ASEV, 50th Anniversary Annual Meeting. pp. 323–336.

Sotelo, J., Benitez, F., Beltran-Heredia, J., Rodriguez, C., 1994. Gas holdup and mass transfer coefficients in bubble columns. 1. porous glass-plate diffussers. International Chemical Engineering 34, 82–91.

Stephanopoulos, G., 1984. Chemical Process Control: An Introduction to Theory and Practice. Prentice-Hall, Englewood Cliffs, New Jersey.

Taguchi, H., Humphrey, A.E., 1966. Dynamic measurement of the volumetric oxygen transfer coefficient in fermentation systems. J. Ferment. Technol. 44, 881–889.

Tobajas, M., Garcia-Calvo, E., 1996. Prediction of hydrodynamic behaviour in bubble columns. Journal of Chemical Technology and Biotechnology 66, 199–205.

Ulbrecht, J.J., Kawase, Y., Auyeung, K.F., 1985. More on Mixing of Viscous Liquids in Bubble Columns. Chem. Eng. Commun. 35, 175–191.

Varela, C., Pizarro, F., Agosin, E., 2004. Biomass Content Governs Fermentation Rate in Nitrogen-Deficient Wine Musts. Society 70, 3392–3400.

Vashitz, O., Sheintuch, M., Ulitzur, S., 1989. Mass transfer studies using cloned-luminous strain of Xanthomonas campestris. Biotechnology and Bioengineering 34, 671–680.

Villadsen, J., Nielsen, J., Lidén, G., 2011. Bioreaction engineering principles. Springer Verlag, New York.

Walker, G., 1998. Yeast Physiology and Biotechnology. John Wiley and Sons.

Wang, M., Tang, S.X., Tan, Z.L., 2011. Modeling in vitro gas production kinetics: Derivation of Logistic–Exponential (LE) equations and comparison of models. Animal Feed Science and Technology 165, 137–150.

Whitman, W., 1923. A preliminary experimental confirmation of the two-film theory of gas absorption. Chem Metal Eng 29, 146–148.

Wilhelm, E., Battino, R., Wilcock, R.J., 1976. Low-Pressure Solubility of Gases in Liquid Water. Chemical Reviews 77, 219–262.

Wu, Y., Al-Dahhan, M.H., 2001. Prediction of axial liquid velocity profile in bubble columns. Chemical Engineering Science 56, 1127–1130.

Wu, Y., Ong, B.C., Al-Dahhan, M., 2001. Predictions of radial gas holdup profiles in bubble column reactors. Chemical Engineering Science 56, 1207–1210.

Zak, D., Stelling, J., Doyleiii, F., 2005. Sensitivity analysis of oscillatory (bio)chemical systems. Computers & Chemical Engineering 29, 663–673.

Çalik, P., Yilgör, P., Ayhan, P., Demir, A.S., Calik, P., Yilgor, P., 2004. Oxygen transfer effects on recombinant benzaldehyde lyase production. Chemical Engineering Science 59, 5075–5083.